Development of a Simulation Methodology for Gas Turbine Combustion

Thommie Nilsson

Supervisors:
Harry Lehtiniemi (LOGE AB)
Cathleen Perlman (LOGE AB)
Daniel Lörstad (SIT AB)
Sven-Inge Möller (Combustion physics, Lund University)

LUND
UNIVERSITY

Master's thesis in physics, 60 p
Lund University, 2014

Abstract

The main goal of this thesis was the development and application of a method to construct reactor networks based on pre-calculated flow fields for combustion systems. Computational fluid dynamics (CFD) was used to calculate flow fields for the Sandia piloted jet flame D and a Siemens SGT-800 gas turbine burner rig. Two different combustion models were tested in the computational fluid dynamics calculations: one based on homogeneous reactor chemistry and the other utilizing a progress variable based conditional moment closure (CMC) combustion model. When applied to the Sandia flame, the homogeneous reactor model was found to compress the flame and overpredict the temperature compared to experimental data but did otherwise show good agreement. With the CMC model, the mixture fraction variance was over-predicted leading to the flame being separated from the burner outlet, a so-called lift-off, otherwise the maximum temperature and OH level were calculated more accurately than with homogeneous reactors.

Two algorithms for reactor network construction were developed and implemented. These two algorithms group computational cells into zones using a principal component analysis (PCA) and a cluster growth method, respectively. Networks were used to study NO formation for varying flame temperature and hydrogen content. Temperature and hydrogen content are parameters which were not varied in the computational fluid dynamics simulations. Network calculations showed reasonable agreement with computational fluid dynamics and experimental results in terms of trends in NO formation and temperature field. The results for the burner rig implies that prompt NO formation is prominent and part of the reason why NO increases with increased hydrogen content.

Networks of partially stirred stochastic reactors were also investigated. Parameter studies showed that the required number of particles vary between reactors but needed not be higher than around 55 for the conditions studied. It was also seen that an optimum value can be found for the stochastic mixing time and near this value the results are better than in corresponding homogeneous reactor networks.

Acknowledgement

I would like to thank everyone who has given me this opportunity and made this thesis possible. I thank Harry Lehtiniemi at LOGE for all the interesting discussions we had, for answering all my questions and explaining so many things about combustion modelling and computational fluid dynamics. I also thank Cathleen Perlman at LOGE for discussions on reactor networks and a lot of help with the computer codes. I thank Daniel Lörstad at SIT for providing data and meshes and for many helpful discussions. I wish to thank Sven-Inge Möller at Lund University for all his support and feedback. I also want to thank Lars Seidel, Anders Borg and Simon Bjerkborn at LOGE for all discussions and the motivation they gave me. I thank Dr. Rajesh Rawat at CD-adapco for providing the STAR-CD license used in this work.

Finally, I want to thank everyone supporting me during this work.

Lund, December 2014
Thommie Nilsson

Publication note

Some of the results presented in this thesis also serve as a source for the paper "Gas Turbine Burner Reactor Network Construction and Application" submitted to the 2015 ICDERS conference.

Lund Reports on Combustion Physics, LRCP-183
ISRN LUTFD2/TFCP-183-SE
ISSN 1102-8718
Lund, Sweden, January 2015
Thommie Nilsson
Division of Combustion Physics
Department of Physics
Faculty of Engineering LTH
Lund University
P.O. Box 118
SE-221 00 Lund, Sweden

Contents

Nomenclature

Symbols

D	Diffusivity [m^2/s], Inlet diameter [m]
h	Enthalpy [J/kg]
h_{298}	Enthalpy of formation at 298 K [J/kg]
I	Interval [:]
k	Turbulent kinetic energy [m^2/s^2]
m	Mass [kg]
p	Pressure [Pa]
P	Probability density [:]
Pr	Prandtl number [:]
Q	Conditionally averaged scalar
R	Gas constant [$J/(mol \cdot K)$], random number [:]
Re	Reynolds number [:]
Sc	Schmidt number [:]
t	Time [s]
T	temperature [K]
v	Velocity [m/s]
V	Volume [m^3]
W	Molar mass [kg/mol]
Y	Species mass fraction [:]
Z	Mixture fraction [:]

Greek symbols

ε	Turbulent dissipation rate [m^2/s^3]
η	Mixture fraction sample space [:]
λ	Thermal conductivity [$J/(K \cdot m \cdot s)$]
μ	Viscosity [$Pa \cdot s$]
ν	Stoichiometric coefficient [:]
ρ	Density [kg/m^3]
τ	Stress tensor [Pa], residence time [s]
τ_{mix}	Mixing time scale [s]
τ_{turb}	Turbulent time scale [s]
χ	Scalar dissipation rate [1/s]
ω	Chemical source term [kg/s]
ω_{h298}	Progress variable soource term [$J/(kg \cdot s)$]

Other symbols

$\bar{}$	Average
$\tilde{}$	Favre average
$\langle\,\rangle$	Conditional average

Abbreviations

CFD	Computational Fluid Dynamics
CMC	Conditional Moment Closure
CPU	Central Processing Unit
DLE	Dry Low Emission
GRI	Gas Research Institute
LTIF	Library of Transient Flamelets
PCA	Principal Component Analysis
PDF	Probability Density Function
PISO	Pressure Implicit with Splitting of Operator
RANS	Reynolds Averaged Navier Stokes
RMS	Root Mean Square
SIT	Siemens Industrial Turbomachinery

1 Introduction

Today gas turbines are popular industrial energy sources for electricity generation. The challenges in developing industrial gas turbines are to achieve high efficiency, low emissions, fuel flexibility, stable operation and long durability [1, 2]. Reliable experimental techniques as well as computer simulations are needed in order to understand and improve combustion technology. Computer simulations are useful to interpolate between measured data and to test new designs, especially since such experiments can be expensive. Simulations are also important for the understanding of phenomena since all information that could be of importance may not be easily measurable.

1.1 The Problem of Modelling Turbulent Combustion

The two main problems in reactive flow simulations are chemical reactions and their interaction with turbulent flows. The problem with reactions themselves is all the different time scales they introduce, known as stiffness. Chemical time scales can typically range from 10^{-10} s for fast reactions involving radicals to 10^{3} s for slow emission formation. The problem with chemistry-turbulence interaction is the small length scales where molecular mixing and chemical reactions take place. For example, the molecular length scale is of the order of nm (10^{-9} m) while the dimensions of a gas flame is of the order 1 m.

Computational fluid dynamics (CFD) is the method of calculating fluid flow on a computer by numerically solving discretized versions of the governing equations. Even in the absence of chemical reactions the presence of turbulence becomes a problem in such calculations. Flow in any practical combustion system, such as a jet flame or an engine, is turbulent and turbulence itself is a complex phenomenon that still today is not fully understood on a fundamental level.

In combustion systems, mixing of fuel, oxidizer, radicals and enthalpy take place on microscopic scales and this mixing interacts with turbulence. Such interaction can be challenging to capture in a computer simulation because the small scales can generally not be resolved in simulations. Simply resolving all scales necessary to perform a direct numerical solution of the governing equations comes at an unrealistically high computational cost (memory and CPU-time) for any large or complex geometry. Using a coarser computational grid is possible if some of the small scale features of the flow are filtered out from the flow equations and modeled by a turbulence model; the solution of such filtered equations is an average flow field and such methods are commonly used for non-reacting flow. There is however a problem if the flow is reactive: the chemical source term is non-linear and can in general not be approximated from averaged quantities transported on a coarse grid. The purpose of a combustion model is to estimate the chemical source term. Several combustion models have been suggested, some major types include flamelet models, conditional moment closure (CMC) models and transported probability density function (PDF) models. These concepts will be explained later. Still today, computer simulations of turbulent reactive flows are far from perfect and there is a need to develop, validate and improve the models to make simulations more reliable. Especially in industrial applications, where the computational time and cost is a concern, the accuracy-to-time/cost ratio is important.

1.2 Aim and Limitations

The Computational fluid dynamics part of the thesis was limited to two-dimensional meshes and the Reynolds averaged Navier-Stokes (RANS) flow equations. This was chosen over more advanced flow calculation methods, like large eddy simulation which is a method that resolves

the large scales of swirling flows (eddys). Such methods would have required a lot more computational time. In this thesis many simulations had to be done to sort out several problems and to compare models. As a result the computational time per simulation was a concern.

The combustion models studied were a homogeneous reactor model and a library of transient flamelets with conditional moment closure (LTIF-CMC) model. The main focus was on homogeneous reactors because these simulations were selected as starting point for the reactor network part of the thesis. Only a brief study of LTIF-CMC was done since higher priority was given to solving flow-related instability problems that occurred.

In the reactor network part of the thesis the priority was the construction method and the use of stochastic reactors. Network calculations were mainly focused on the Siemens burner rig. This choice was made because the recirculating flow make the rig less dependent on turbulent upstream transport. Since such only net flows were included in the reactor network calculations in this thesis the burner rig turned out to be more suitable for these reactor networks as will be discussed later.

The main objectives of this thesis are:

- Evaluate the LTIF-CMC combustion model for methane flames in computational fluid dynamics simulations with RANS and k-ε turbulence modelling.
- Develop a method to derive a reactor network from a computational fluid dynamics simulation and evaluate the performance of such a network.
- Evaluate stochastic reactor networks for methane burners.
- Apply the LTIF-CMC and homogeneous reactor computational fluid dynamics models and the reactor network to an academic test case (Sandia flame D).
- Apply the LTIF-CMC and homogeneous reactor computational fluid dynamics models and the reactor network to an industrial case (the SGT-800 burner in Siemens atmospheric combustion rig).

1.3 Thesis Structure

In section 2 the theory is outlined, important concepts and models are explained and the simulated experiments are described. Previous works are discussed at the end of this section. Section 3 explains the model development done in this thesis. This mainly concerns the construction algorithm for reactor networks but also extensions made to existing CMC and reactor network codes. In section 4 simulation set-ups are described in detail and the results are presented and discussed. In section 5 a summary of results and conclusions are given. In Figure 1 the structure of the work presented in this thesis is shown.

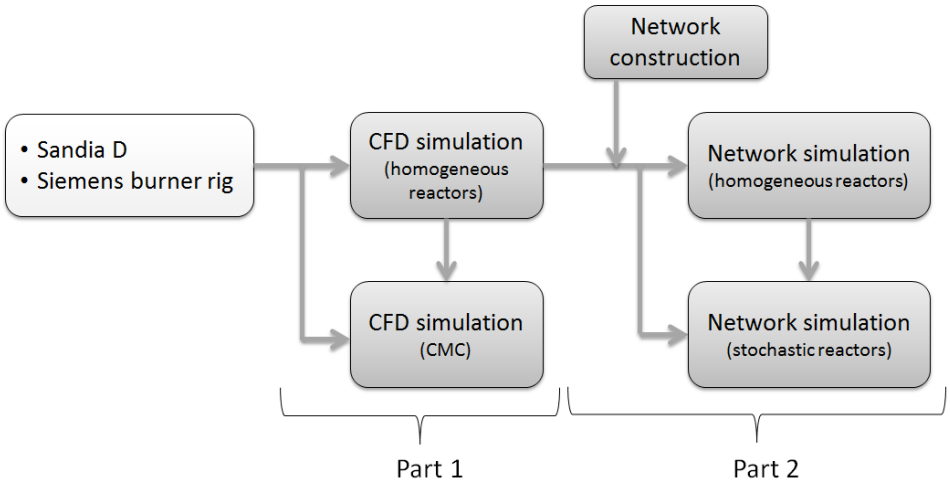

Figure 1: Overview of the work done in this thesis. The first part is about computational fluid dynamics and the second part is about reactor networks.

2 Background and Theory

This section begins with a general description of the governing equations of chemically reacting flow. Then follow descriptions of some concepts central to this work: computational fluid dynamics (CFD) using Reynolds averaged Navier-Stokes (RANS), the CMC combustion model, the concepts of homogeneous reactors and their use in computational fluid dynamics and the concept of stochastic reactors. A short description of the experimental setups subject to modelling is given and the section ends with a discussion of previous works in the field.

2.1 Fluid Dynamics and Reactive Flow

The governing balance equations for quantities that describe the flow field can be written as a set of partial differential equations (1-4), see for example Peters [3] and Poinsot [4]. The first equation comes from the conservation of mass. The second equation describe the balance of momentum and has source terms for pressure gradients and viscosity. The third equations describe the balance of enthalpy and has sources for compression, expansion conduction and diffusion. The last equation describe chemical species and has source terms for diffusion and chemical reactions. In the following equations summation is implied for indexes i, j and k when repeated.

$$\frac{\partial \rho}{\partial t} + \frac{\partial}{\partial x_i}(\rho v_i) = 0 \tag{1}$$

$$\frac{\partial \rho v_i}{\partial t} + \frac{\partial}{\partial x_j}(\rho v_j v_i) = -\frac{\partial p}{\partial x_i} + \frac{\partial \tau_{ji}}{\partial x_j} \tag{2}$$

$$\frac{\partial \rho h}{\partial t} + \frac{\partial}{\partial x_i}(\rho v_i h) = \frac{\partial p}{\partial t} + v_i \frac{\partial p}{\partial x_i} + \frac{\partial}{\partial x_i}\left(\lambda \frac{\partial T}{\partial x_i}\right) + \frac{\partial}{\partial x_i}\left(\sum_{\alpha=1}^{n} h_\alpha \rho D_\alpha \frac{\partial Y_\alpha}{\partial x_i}\right) \tag{3}$$

$$\frac{\partial \rho Y_\alpha}{\partial t} + \frac{\partial}{\partial x_i}(\rho v_i Y_\alpha) = \frac{\partial}{\partial x_i}\left(\rho D_\alpha \frac{\partial Y_\alpha}{\partial x_i})\right) + \omega_\alpha \tag{4}$$

Here, n is the number of species, $\tau_{ij} = \mu(2S_{ij} - \frac{2}{3}\delta_{ij}\frac{\partial v_k}{\partial x_k})$ is the viscous stress tensor with

$$S_{ij} = \frac{1}{2}\left(\frac{\partial v_i}{\partial x_j} + \frac{\partial v_j}{\partial x_i}\right) \tag{5}$$

and D_α is the diffusivity of species α. Frictional heating and radiation have been neglected in the enthalpy equation and gravity is neglected in the momentum equation. The mass fractions Y_α must obey the condition $\sum_\alpha Y_\alpha = 1$ and the sum of equations (4) should equal equation (1) so that one of the mass fractions need not be solved for. In the models used in this thesis, however, all mass fractions are always solved for.

The term ω_α is the source of species α due to chemical reactions. It contains one term for each reaction where the species α participate and each term is proportional to the stoichiometric coefficient of α (the sign depend on α being a reactant or product) and the rate of the reaction. For a set of R reactions the chemical sources are given by [3]

$$\omega_\alpha = W_\alpha \sum_{r=1}^{R} \nu_{\alpha r} \left(k_r^f \prod_{\beta=1}^{n} \left(\frac{\rho Y_\beta}{W_\beta} \right)^{\gamma_{\beta r}^f} - k_r^b \prod_{\beta=1}^{n} \left(\frac{\rho Y_\beta}{W_\beta} \right)^{\gamma_{\beta r}^b} \right) \tag{6}$$

where the index r runs over all reactions, the superscripts f and b denote forward and backward reaction, W_α is the molar mass (kg/mol) of species α and $\nu_{\alpha r}$ is the net stoichiometric coefficient of species α in reaction r. $\gamma_{\beta r}^f$ and $\gamma_{\beta r}^b$ are the forward and backward orders of reaction r with respect to species β. The reaction rates k_r are modeled by the Arrhenius law as

$$k_r = A_r T^{n_r} e^{-E_r/(RT)} \tag{7}$$

The equations just described form the basis of reactive flow. But, in order to do numerical computations some coarse graining of these equations is typically needed. So called Reynolds filtering is one such method and it is described in the next section.

2.2 Computational Fluid Dynamics and Reynolds Filtering

For applications where the Reynolds number is high the solution to equations (1-7) becomes chaotic, which is known as turbulence. Reynolds number $\mathrm{Re} = \frac{\rho v D}{\mu}$, is the ratio of inertia to viscosity with D being a typical length scale over which the velocity changes. A high Reynolds number essentially means that the viscous forces are not strong enough to quickly damp perturbations in the velocity field.

In the case of turbulent flow it is not practical to solve the equations (1-7) directly, not even in the absence of chemical reactions. The reason for this is that the length scale of the smallest eddy currents, known as the Kolmogorov scale, is so small that the required resolution of the computational mesh becomes too expensive to use. The direct numerical solution of (1-7) is only applicable to very small and simple geometries in case of turbulent flow; in most practical cases the equations have to be filtered in order to be usable on a coarse mesh.

The method used for flow calculations in this work is based on the so called RANS equations, which are obtained by decomposing density, velocity components, enthalpy and mass fractions into mean values and fluctuations: $f = \bar{f} + f'$. A Reynolds averaged quantity (denoted by $\bar{}$) is a time or ensemble average. For reactive flows, large density fluctuations are to be expected and mass weighted so called Favre averages are commonly used instead of Reynolds averages. A quantity f is then decomposed into an average and a fluctuation: $f = \widetilde{f} + f''$ [3]. The fluctuations, both f' and f'', are assumed to have zero mean: $\bar{f}' = 0$ and $\widetilde{f''} = 0$. A Favre average (denoted by $\tilde{}$) is defined as

$$\widetilde{f} = \frac{\overline{\rho f}}{\bar{\rho}} \tag{8}$$

By applying a Reynolds average to each term in the balance equations, decomposing the principal variables into Favre means and fluctuations, using (8) and the fact that fluctuations

have zero mean gives the RANS equations for the averaged quantities [4] (summation is implied for indexes i, j and k when repeated):

$$\frac{\partial \bar{\rho}}{\partial t} + \frac{\partial}{\partial x_i}(\bar{\rho}\tilde{v}_i) = 0 \tag{9}$$

$$\frac{\partial \bar{\rho}\widetilde{v_i}}{\partial t} + \frac{\partial}{\partial x_j}\left(\bar{\rho}\widetilde{v_j}\widetilde{v_i}\right) = -\frac{\partial \bar{p}}{\partial x_i} + \frac{\partial}{\partial x_j}\left(\overline{\tau_{ji}} - \bar{\rho}\widetilde{v_j''v_i''}\right) \tag{10}$$

$$\frac{\partial \bar{\rho}\widetilde{h}}{\partial t} + \frac{\partial}{\partial x_i}(\bar{\rho}\widetilde{v_i}\widetilde{h}) = \frac{\partial \bar{p}}{\partial t} + \widetilde{v_i}\frac{\partial \bar{p}}{\partial x_i} + \overline{v_i''\frac{\partial p}{\partial x_i}} + \frac{\partial}{\partial x_i}\left(\overline{\lambda\frac{\partial T}{\partial x_i}} + \overline{\sum_{\alpha=1}^{n} h_\alpha \rho D_\alpha \frac{\partial Y_\alpha}{\partial x_i}} - \bar{\rho}\widetilde{v_i''h''}\right) \tag{11}$$

$$\frac{\partial \bar{\rho}\tilde{Y}_\alpha}{\partial t} + \frac{\partial}{\partial x_i}(\bar{\rho}\tilde{v}_i\tilde{Y}_\alpha) = \frac{\partial}{\partial x_i}\left(\overline{\rho D_\alpha \frac{\partial Y_\alpha}{\partial x_i}} - \bar{\rho}\widetilde{v_i''Y_\alpha''}\right) + \overline{\omega_\alpha} \tag{12}$$

Correlations between fluctuations of different quantities appear in these averaged equations; these correlation terms are unknown and need to be modeled in order to close the equations. There are correlations between fluctuating velocity components $\widetilde{v_i''v_j''}$ (known as Reynolds stresses) and the turbulent fluxes of species and enthalpy, $\widetilde{v_i''Y_\alpha''}$ and $\widetilde{v_i''h''}$.

Turbulent mass fraction and enthalpy fluxes are closed by gradient transport assumptions. This means that the turbulent fluxes are treated as extra diffusion terms:

$$\bar{\rho}\widetilde{v_i''Y_\alpha''} = -\frac{\mu_t}{\mathrm{Sc}_\alpha}\frac{\partial \tilde{Y}_\alpha}{\partial x_i} \tag{13}$$

$$\bar{\rho}\widetilde{v_i''h''} = -\frac{\mu_t}{\mathrm{Pr}_h}\frac{\partial h}{\partial x_i} \tag{14}$$

The average molecular diffusion terms in (11) and (12) are modeled by using the average of each factor instead of the whole term:

$$\overline{\rho D_\alpha \frac{\partial Y_\alpha}{\partial x_i}} = \bar{\rho} D_\alpha \frac{\partial \tilde{Y}_\alpha}{\partial x_i} \tag{15}$$

In turbulent systems molecular diffusion is typically very small compared to turbulent transport. For example, in the simulations performed in this thesis values of μ_t are typically greater than 10^{-3}. With the constants given in Table 1 and the density $\rho \approx 1$ the pre-factors become $\mu_t/Sc_\alpha \approx 10^{-3}$ for the turbulent transport term and $\rho D_\alpha \approx 10^{-5}$ for the molecular transport term so the difference is a factor of order 100 indicating that molecular diffusion is of no importance for these systems.

The Reynolds stresses are closed by introducing a model of turbulence; in this thesis the k-ε model and the Reynolds stress model are used. These two models will now be briefly described.

In the k-ε model the Reynolds stresses are modeled as additional viscous damping by the Boussinesq eddy viscosity approximation:

$$\bar{\rho}\widetilde{v_j''v_i''} = -\mu_t\left(\frac{\partial \widetilde{v_i}}{\partial x_j} + \frac{\partial \widetilde{v_j}}{\partial x_i} - \frac{2}{3}\delta_{ij}\frac{\partial \widetilde{v_k}}{\partial x_k}\right) + \frac{2}{3}\bar{\rho}\tilde{k}\delta_{ij} \tag{16}$$

Here, k is the turbulent kinetic energy, defined as $k = \widetilde{v_i''v_i''}/2$ and the turbulent viscosity, μ_t, is defined as

$$\mu_t = \frac{C_\mu \bar{\rho}\tilde{k}^2}{\tilde{\varepsilon}} \tag{17}$$

Table 1: Model constants used in computational fluid dynamics simulations.

D_α	$3.004 \cdot 10^{-5}$ m^2/s
Sc_α	0.9
Sc_Z	0.9
$\mathrm{Sc}_{Z''^2}$	0.9
Pr_h	0.9
Pr_k	1.0
Pr_ε	1.219
C_μ	0.09
$C_{\varepsilon 1}$	1.44
$C_{\varepsilon 2}$	1.92
$C_{\varepsilon 3}$	1.44
$C_{\varepsilon 4}$	-0.33

The decay rate of k is described by the turbulent dissipation rate ε. Transport equations for the turbulent kinetic energy and its dissipation rate are [5]

$$\frac{\partial \bar{\rho}\tilde{k}}{\partial t} + \frac{\partial \bar{\rho}\tilde{v}_j\tilde{k}}{\partial x_j} = \frac{\partial}{\partial x_j}\left(\mu + \frac{\mu_t}{\mathrm{Pr}_k}\right)\frac{\partial \tilde{k}}{\partial x_j} + \mu_t P - \bar{\rho}\tilde{\varepsilon} - \frac{2}{3}\left(\mu_t \frac{\partial \tilde{v}_i}{\partial x_i} + \bar{\rho}\tilde{k}\right)\frac{\partial \tilde{v}_i}{\partial x_i} \tag{18}$$

$$\frac{\partial \bar{\rho}\tilde{\varepsilon}}{\partial t} + \frac{\partial \bar{\rho}\tilde{v}_j\tilde{\varepsilon}}{\partial x_j} = \frac{\partial(\mu + \frac{\mu_t}{\mathrm{Pr}_\varepsilon})}{\partial x_j}\frac{\partial \tilde{\varepsilon}}{\partial x_j} + C_{\varepsilon 1}\frac{\tilde{\varepsilon}}{\tilde{k}}\left(\mu_t P - \frac{2}{3}(\mu_t \frac{\partial \tilde{v}_i}{\partial x_i} + \bar{\rho}\tilde{k})\frac{\partial \tilde{v}_i}{\partial x_i}\right) + C_{\varepsilon 2}\bar{\rho}\frac{\tilde{\varepsilon}^2}{\tilde{k}} + C_{\varepsilon 4}\bar{\rho}\tilde{\varepsilon}\frac{\partial \tilde{v}_i}{\partial x_i} \tag{19}$$

where

$$P = 2S_{ij}\frac{\partial \tilde{v}_i}{\partial x_j} \tag{20}$$

and S_{ij} is given by equation (5). The relevant model constants are summarised in Table 1. All constants related to the k-ε turbulence model have their standard values.

The other turbulence model used in this work is the Reynolds stress model. The main feature of this model is that the Reynolds stresses $\widetilde{v_i'' v_j''}$ are transported as field variables, which is done according to the following transport equation:

$$\frac{\partial \bar{\rho}\widetilde{v_i'' v_j''}}{\partial t} + \frac{\partial v_k \bar{\rho}\widetilde{v_i'' v_j''}}{\partial x_k} = D_{ij} - \bar{\rho}\left(\widetilde{v_i'' v_k''}\frac{\partial v_j}{\partial x_k} + \widetilde{v_j'' v_k''}\frac{\partial v_i}{\partial x_k}\right) + \overline{p''\left(\frac{\partial v_i}{\partial x_j} + \frac{\partial v_j}{\partial x_i}\right)} - \bar{\rho}\frac{2}{3}\delta_{ij}\varepsilon \tag{21}$$

where $D_{ij} = \frac{\partial}{\partial x_k}\left(-\bar{\rho}\widetilde{v_i'' v_j'' v_k''} - \delta_{ik}\widetilde{p'' v_j''} - \delta_{jk}\widetilde{p'' v_i''} + \mu\delta_{kl}\frac{\partial}{\partial x_l}\widetilde{v_i'' v_j''}\right)$ is a diffusion term, the second term on the right corresponds to production and the fourth term on the right corresponds to dissipation where ε is obtained in a way similar to that of the k-ε model. The third term on the right involves pressure fluctuations and needs to be approximated. The Reynolds stress model contains more transport equations and has a higher computational cost than the k-ε model.

The computational fluid dynamics models is not discussed further here. More details on the implementation and modelling assumptions can be found in [5].

2.2.1 Enthalpy and Mixture Fraction

In all simulations in this thesis the heat capacity at constant pressure, $c_p(T)$, of any species is described as a polynomial function of temperature. The polynomial coefficients for each species are part of the chemical reaction scheme. The static enthalpy, $h(T)$, which is transported according to (11), is the integral of $c_p(T)$ for each species and, under the assumption that the

mixture is an ideal gas, these integrals are also polynomials and the enthalpy of a mixture is the mass weighted sum of individual species enthalpies. Temperatures are calculated by inverting the polynomial functions numerically.

A field variable that requires some extra attention is the mixture fraction, Z. It is a passive conserved scalar, meaning that it does not have a source term. Its transport equation is

$$\frac{\partial \bar{\rho}\tilde{Z}}{\partial t} + \frac{\partial}{\partial x_i}(\bar{\rho}\tilde{v}_i\tilde{Z}) = \frac{\partial}{\partial x_i}\left(\overline{\rho D_Z \frac{\partial Z}{\partial x_i}} - \bar{\rho}\widetilde{v_i'' Z''}\right) \tag{22}$$

The transported mixture fraction is defined as the fraction of gas originating from a particular inlet: $Z = \frac{m_1}{m_1+m_2}$ where m_1 and m_2 are the masses originating from inlet 1 and 2, usually corresponding to fuel and oxidizer, respectively. This kind of mixture fraction is commonly used by combustion models that do not track individual species, like the LTIF-CMC which is described in section 2.3.

The variance of mixture fraction, $\widetilde{Z''^2}$, is also used by the LTIF-CMC model and its transport equation is [3]

$$\rho\frac{\partial \widetilde{Z''^2}}{\partial t} + \rho v_i \frac{\partial \widetilde{Z''^2}}{\partial x_i} = -\frac{\partial}{\partial x_i}\left(\rho\widetilde{v_i'' Z''^2}\right) - 2\frac{\mu_t}{\mathrm{Sc}_{Z''^2}}\left(\nabla\widetilde{Z}\right)^2 - \rho\widetilde{\chi} \tag{23}$$

where μ_t = is the turbulent viscosity (defined by equation 17) and $\chi \equiv 2D_Z(\nabla Z)^2$ is the scalar dissipation rate. The Favre average of the squared gradient is not available. The scalar dissipation rate is instead modeled as [3] $\chi = C_\chi \cdot \varepsilon\widetilde{Z''^2}/k$. The model constant C_χ is a ratio between transport in η-space and transport at the integral length scale of the turbulence model and has the standard value 2 [3]. A gradient assumption similar to equations (13-14) is used to close the flux term $\widetilde{v_i'' Z''^2}$.

2.3 LTIF-CMC Combustion Model

As mentioned in the introduction, the problem when computing reactive flow is that chemical reactions occur on very small scales and at widely varying rates. If the flow is turbulent the RANS equations only provide mean values of field variables for each cell and this may be too coarse a scale to resolve the effects of chemistry directly. In a turbulent non-premixed flame for example, the combustion reactions happen in a very thin reaction layer where the fuel, oxidizer and radicals mix. Since the flame is not premixed there will be a variety of fuel/oxidizer mixture fractions present in every computational cell. The chemical source term in a cell should be calculated as the average of source terms at all (unresolved) conditions present in the cell. Just using the average cell condition provided by the RANS solution is not enough due to the non-linearity of chemical sources. This can be expressed as

$$\bar{\omega} \neq \omega(\tilde{Y}, \bar{p}, \tilde{T}) \tag{24}$$

The basic assumption of CMC is that fluctuations of different quantities are correlated. As a consequence any conditioned quantity $\langle\psi|\eta\rangle$ fluctuates less than ψ itself.

A quantity ξ that fluctuates strongly at sub-grid (unresolved) scales is chosen for conditioning, for non-premixed combustion mixture fraction is a natural choice. A sample space variable of ξ is denoted η. Unconditioned averaged quantities $\widetilde{\psi}$ that appear in the RANS equations are replaced by conditioned averages $\langle\psi(t,x_i)|\widetilde{\xi(t,x_i)} = \eta\rangle$, which have smaller fluctuations than their unconditional counterparts. This means that η is treated as an additional independent variable that has to be discretized and all quantities have to be resolved not only spatially and

temporally but also in η-space. An instantaneous value of the quantity ψ in one point in space can be decomposed into a conditional mean and fluctuation:

$$\psi(x,t) = \langle \widetilde{\psi(x,t)} | \eta \rangle + \varphi$$

where the fluctuation φ about the conditional mean is assumed to be small.

A probability density function (PDF) resolved on the η-grid, $P(\eta)$, describes the probability of finding $\xi = \eta$. The PDF is assumed to follow a beta distribution between 0 and 1:

$$P(\eta; \alpha, \beta) = C\eta^{\alpha-1}(1-\eta)^{\beta-1}$$

where $C = \int_0^1 \eta^{\alpha-1}(1-\eta)^{\beta-1} d\eta$ is a normalization constant. Parameters α and β in each cell are determined from the unconditional mean and variance of mixture fraction according to

$$\alpha = Z\left(\frac{Z(1-Z)}{Z''^2} - 1\right)$$

$$\beta = (1-Z)\left(\frac{Z(1-Z)}{Z''^2} - 1\right)$$

Quantities Y_α described by equation (4) are referred to as reactive scalars and transport of their Favre averaged conditional versions

$$Q_\alpha = \frac{\langle \rho Y_\alpha | \eta \rangle}{\langle \rho | \eta \rangle} \tag{25}$$

is described by the CMC equation:

$$\frac{\partial Q_\alpha}{\partial t} + \langle v_i | \eta \rangle \frac{\partial Q_\alpha}{\partial x_i} + \frac{\frac{\partial}{\partial x_i}\left(\langle v_i'' Y_\alpha'' | \eta \rangle \tilde{P}(\eta)\right)}{\tilde{P}(\eta)\bar{\rho}} = \frac{\langle \chi | \eta \rangle}{2} \frac{\partial^2 Q_\alpha}{\partial \eta^2} + \langle \omega_\alpha | \eta \rangle \tag{26}$$

where $\tilde{P}(\eta) = \langle \rho | \eta \rangle P(\eta)/\bar{\rho}$ is the Favre averaged PDF.

A detailed derivation of the CMC equation is given by Klimenko and Bilger [6]. In practice, conditional variables are represented by choosing a discretization of η and transporting multiple versions of the conditioned variable, one for each point on the η-grid.

Conditional velocity is assumed equal to the unconditional value, $\langle \boldsymbol{v} | \eta \rangle = \tilde{\boldsymbol{v}}$ and conditional turbulent fluxes $\langle v_i'' Y_\alpha'' | \eta \rangle$ are modeled using a gradient transport assumption of the same form as equation 13. Conditional scalar dissipation is assumed to follow an inverse complementary error function in η-space. The conditional source term is closed to first order using the flamelet table described in section 2.3.1. Further details on these assumptions are given in [7].

The conditional quantities Q_α could be conditional versions of the mass fractions. However, due to the large number of species, a single conditioned progress variable is instead transported in the LTIF-CMC model. A progress variable is a bounded quantity that indicates how far the chemical reactions have progressed; the highest and lowest possible values corresponds to reactants (fuel and oxidizer) and products (chemical equilibrium), respectively. The conditional progress variable is evaluated on the same spatial grid as the flow. If conditional mass fractions were to be transported, however, it is common to use a coarser spatial grid for the conditional variables but that approach is not taken in this work. The progress variable used here is the enthalpy of formation at 298 K, $Q = h_{298}$. Enthalpy of formation is also described by the CMC equation (26). In literature 298 K is the standard temperature for reporting thermodynamic quantities. Enthalpy of formation is not the only possible choice of progress variable; other possibilities include for example product mass fractions or linear combinations thereof. It is

required of a progress variable to be strictly increasing (or decreasing) throughout the reaction progress. This constraint ensures the existence of an invertible mapping between the progress variable and time (in a closed system). If a combination of mass fractions is to be used it thus has to be chosen carefully to make sure this is fulfilled. A disadvantage of enthalpy of formation as conditional progress variable is that it may increase a bit right at the beginning of combustion where endothermic reactions happen before it starts to decrease. This initial phase is very short and can be neglected, this is treated during table generation. The obvious choice of using entropy as progress variable is not suitable because entropy is not described fully by equation (4), it needs additional terms to account for its dependence on mixing.

The highest possible value of h_{298} corresponds to an unburned mixture while the lowest value corresponds to a completely burned mixture. The range of values accessible to the progress variable (and the corresponding chemical compositions) depends on mixture fraction. Species mass fractions thus become functions of η and h_{298} and the averages can be computed as

$$\widetilde{Y_k} = \int_0^1 Y_k(\eta, h_{298}, \chi) P(\eta) d\eta$$

Note however that it is not required to know any mass fractions for the computational fluid dynamics computation; it is enough to know the thermal properties and the source term, ω_{h298} representing ω in equation (26), as functions of η and h_{298} to perform the computation. Mass fractions are only calculated for post-processing purposes.

2.3.1 Flamelet Table

Computing chemical source terms for each grid point in mixture fraction-space during the course of a computational fluid dynamics simulation with CMC would be very expensive in terms of CPU time. The two terms on the right hand side of equation (26) are essentially identical to what appears in flamelet equations and thus these terms are modeled by flamelets, which can be pre-calculated and stored in a table. The tabulation procedure is described in [8] and will not be reported here.

A flamelet is a one-dimensional construct resolved in mixture fraction-space. In a non-premixed flame consider a surface of constant mixture fraction $Z = \eta$. It is possible to define a coordinate transform $(t, x_1, x_2, x_3) \rightarrow (\tau, Z, Z_2, Z_3)$ where Z is the mixture fraction coordinate, which is always normal to the surface, and Z_2 and Z_3 are coordinates in directions that span the surface. If the gradient is large it is enough to consider the Z-direction. The other two directions are neglected. The transform means that mixture fraction is treated as an independent variable and the resulting one-dimensional flame in Z-t-space is known as a flamelet. More details are given for example in [4] and [3]. Assuming there is no compression or expansion the resulting flamelet equations to solve are

$$\rho \frac{\partial Y_k}{\partial t} = \rho \frac{\chi}{2} \frac{\partial^2 Y_k}{\partial Z^2} + \omega_k \tag{27}$$

$$\rho \frac{\partial h}{\partial t} = \rho \frac{\chi}{2} \frac{\partial^2 h}{\partial Z^2} \tag{28}$$

where the scalar dissipation rate is $\chi = 2D_Z \left(\frac{\partial Z}{\partial x}\right)^2$ and t is the flamelet time. Flamelets are pre-calculated for a given range of pressures and scalar dissipation rates and the progress variable-resolved source terms and thermal data are stored in a table. During the computational fluid dynamics simulation, given mixture fraction, progress variable, pressure, temperature and mean scalar dissipation rate, the table provides the source term for the progress variable, the mean molar mass, the polynomial coefficients needed to compute the new temperature and optionally any desired mass fractions.

2.3.2 Temperature Calculation

In this section the calculation of temperature in the CMC model is described. Static enthalpy is not affected by chemical reactions so under the assumption of unity Lewis number (thermal and mass diffusivities equal) and no radiation, enthalpy is a linear function in mixture fraction space, $h(\eta) = h_{ox} + (h_{fuel} - h_{ox})\eta$. The fuel enthalpy h_{fuel} is constant because the fuel temperature and composition is constant. In the presence of compression effects, h_{ox} cannot be constant but when the unconditional average $\tilde{h}$ is known it can be calculated. To see this, consider $\tilde{h}(\tilde{Z})$:

$$\tilde{h}(\tilde{Z}) = \int_0^1 (h_{ox} + \eta(h_{fuel} - h_{ox}))\tilde{P}(\eta)d\eta \tag{29}$$

A beta PDF has the property that the integral of a polynomial multiplied by the PDF is the polynomial evaluated at the mean of the PDF. Using this gives

$$\tilde{h}(\tilde{Z}) = h_{ox} + \tilde{Z}(h_{fuel} - h_{ox}) \tag{30}$$

from which h_{ox} can be calculated. With the function $\tilde{h}(\tilde{Z})$ known the temperature is then calculated by inverting $\tilde{h}$, which is performed with a polynomial function retrieved from the flamelet table.

2.4 Homogeneous Reactors

One of the simplest combustion models used in computational fluid dynamics is to consider each cell to be a so called homogeneous reactor. This method will be referred to as the homogeneous reactor chemistry method and it was applied to both the Sandia D flame and the Siemens burner rig in this thesis. The disadvantage of homogeneous reactor chemistry is that there is no account for sub-grid scales and chemistry-turbulence interaction. Homogeneous reactors were also used in reactor networks in the second part of this thesis.

A homogeneous reactor is an idealised reactor in which all gases are perfectly mixed at all times. Therefore no momentum equation is required and the transport equations for species and enthalpy are considerably simplified. Constant pressure or constant volume is normally assumed. A homogeneous reactor can be run either in "batch mode" or with a constant inlet stream. Batch mode means that the in- and outflow is completely separated from the advancement of chemical reactions by operator splitting; flow and chemistry are advanced alternately and, since these two steps are usually in opposite directions in composition space, a short time step is required. What is meant by constant inlet is that a source term is added to the species and enthalpy equations that account for inflow. This inflow has constant composition during a solution step but may change between steps.

The species equation for the constant inlet homogeneous reactor is, assuming equal in- and outflow,

$$\frac{\partial Y_\alpha}{\partial t} = \frac{\omega_\alpha W_\alpha}{\rho} + \frac{1}{\tau}(Y_{\alpha,in} - Y_\alpha) \tag{31}$$

where Y_α are mass fractions in the reactor (equal to those at the reactor outlet), $Y_{\alpha,in}$ are mass fractions at the inlet and ω_α are chemical source terms according to equation (6). The residence time $\tau = m/\dot{m}$ is the time it takes for an amount of mass equal to that inside the reactor to flow through, where m is the reactor mass and $\dot{m}$ is the mass influx.

Other common names for homogeneous reactors seen in the literature are well-stirred reactor, perfectly stirred reactor and continuously stirred tank reactor.

When homogeneous reactors are used in computational fluid dynamics every cell is treated as one constant-pressure reactor run in batch mode. Chemical reactions are solved directly using a detailed reaction scheme. Exchange of mass with neighbouring cells is done only during flow steps.

2.5 Stochastic Reactors

Stochastic reactors are used in the reactor network part of this thesis. The stochastic reactor differs from the homogeneous one in two ways: it is partially stirred instead of perfectly stirred and its time evolution is stochastic rather than deterministic. Being partially stirred means that the reactor contains a distribution in all properties, such as temperature and mass fractions, instead of just the average state. This property is useful for example if there are multiple inlets where each inlet stream is different or when an inlet stream itself is not perfectly mixed.

In a stochastic reactor, a discrete realization of the joint PDF of chemical states (enthalpy and mass fractions) is represented by a set of particles. The evolution of the PDF is modeled by integrating the chemistry in each particle on its own and by particle interaction (mixing). This interaction is carried out by a mixing model; in this thesis the Curl model and the modified Curl model are used [9, 10]. In both of these models one mixing event involves mixing of two randomly selected particles. The difference is that in the Curl model the particles are mixed completely so that they both take their common mean, while in the modified Curl model the extent of mixing is decided by another random number. The advantage of modified Curl over Curl is that it produces a continuous PDF [11].

The time between mixing events is controlled by the mixing time, τ_{mix}. For the Curl model the time is given by

$$t_{event} = \frac{\ln(1/R)}{n} \cdot \tau_{mix} \tag{32}$$

where n is the number of particles and R is a random number drawn uniformly on $(0, 1)$. The question is how τ_{mix} should be estimated.

The time scale of turbulent mixing in computational fluid dynamics using RANS is $\tau_{turb} = \ell_I/v' = k/\varepsilon$ where ℓ_I is the integral length scale, v' is the magnitude of velocity fluctuations at the integral length scale, k is turbulent kinetic energy and ε is turbulent dissipation rate. In this thesis, stochastic reactors are used to represent zones of a mesh also used for a computational fluid dynamics simulation, so k and ε for a zone can be extracted from the corresponding cells to give τ_{turb}. Usually the relation

$$\tau_{mix} = \tau_{turb}/C_\phi \tag{33}$$

between the time scales is assumed in transported PDF methods, see for example Pope [9]. The model constant C_ϕ is not known, the value 2 is suggested in [12], which is the same constant, $C_\chi = 2$, used to relate scalar dissipation for flamelets to τ_{turb} as mentioned in section 2.3.1. It is shown in [10] that the constant C_ϕ should be a factor 3/2 larger giving 3/2 as many mixing events when modified Curl is used in order to give the same variance decay rate as in Curl. In this thesis whenever modified Curl is used the corresponding C_ϕ is implicitly multiplied by that factor. This is done in order to easily compare the two mixing models by making a given value of C_ϕ always correspond to the same variance decay rate independent of mixing model.

A stochastic reactor is similar to what is done in particle-based transported PDF methods but in a stochastic reactor no flow is solved and particles do not have a velocity or position. When stochastic reactors are put together to form a network the particles have approximate positions through the knowledge of which reactors they belong to. Networks are discussed further in section 3.2.

2.6 Sandia Flames

Some of the simplest turbulent combustion processes are turbulent jet flames. The Sandia flames C, D, E and F from Sandia National Laboratories [13] are a series of such flames with varying Reynolds number that have been subject to extensive experimental measurements and

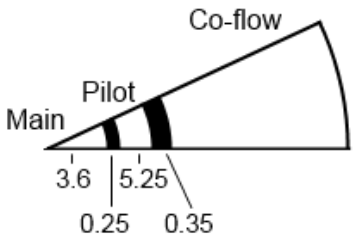

Figure 2: Sector of the cylindrically symmetric Sandia burner. Distances are in millimetres.

modeling, and so they provide a validation test for combustion models. The Sandia flames are part of the subject of this thesis and have been chosen because of the availability of extensive measurement data of several species but also because of the simple geometry, the use of gaseous methane fuel which is rather simple to model and the lack of walls, keeping the number of phenomena to model at a minimum. Flame F in particular is known to be challenging to model since it is very close to complete extinction and local extinction and re-ignition are prominent.

The Sandia burner is an annular piloted premixed jet burner, which produces a main jet of premixed fuel and air surrounded by a pre-burned pilot flame. A sector of the cylindrically symmetric geometry is shown in Figure 2. The pilot provides hot gases in order to stabilize the main flame and a co-flow provides a steady upwards air stream. The burner is operated at atmospheric pressure. Some data on the Sandia flames is summarized in Table 2. Experimental mass fractions are reported for species N_2, O_2, H_2O, H_2, CH_4, CO, CO_2, OH and NO. Reported experimental mixture fractions (fuel-to-air ratios) follow the definition

$$Z = \frac{0.5\left(Y_H - Y_H^0\right)/W_H + 2\left(Y_C - Y_C^0\right)/W_C}{0.5\left(Y_H^1 - Y_H^0\right)/W_H + 2\left(Y_C^1 - Y_C^0\right)/W_C} \tag{34}$$

where Y are elemental mass fractions, W are atomic weights and superscripts 0 and 1 denote co-flow and main inlet conditions, respectively [13].

2.7 Siemens Burner Rig

The SGT-800 is a dry low emission (DLE) gas turbine manufactured by Siemens Industrial Turbomachinery (SIT), which uses a serial cooled annular combustion chamber and 30 burners [14, 15]. The atmospheric combustion rig at SIT, where DLE burners may be tested individually at atmospheric pressure, is made to resemble the SGT-800 combustor. The rig is a subject of simulations in this thesis and is shown in Figure 3 and described in [2]. For confidentiality reasons, all plots of the burner geometry are stretched and all temperature, species and velocity data are given on a relative scale.

2.8 Previous Works

2.8.1 Sandia Flames

The Sandia flames have been modeled many times. Some examples follow. Xu and Pope [16] applied a joint PDF model to flames D, E and F and the method predicts statistics conditional on mixture fraction well. The model in [16] makes use of Lagrangian particles to represent the joint PDF, which is very different compared to the conditional moment closure used in this thesis but there are some similarities with the stochastic reactor model applied in reactor networks in this thesis. The inclusion of two-carbon species in the mechanism is also pointed out as an important factor as is micro mixing to capture local extinction and re-ignition.

Table 2: Sandia flames data summary.

Main inlet radius	3.6 mm
Main-pilot wall	0.25 mm
Pilot thickness	5.25 mm
Outer wall	0.35 mm
Main mass fractions	CH_4 0.1563 O_2 0.1965 N_2 0.6472
Pilot mass fractions	CO_2 0.117 H_2O 0.095 O_2 0.054 N_2 0.734
Co-flow mass fractions	O_2 0.233 N_2 0.767
Main inlet temperature	294 K
Pilot temperature	1880 K
Co-flow temperature	291 K
Pressure	1.0 bar
Main inlet velocity (D)	49.6 m/s
Main inlet velocity (F)	99.2 m/s
Pilot velocity (D)	11.4 m/s
Pilot velocity (F)	22.8 m/s
Pilot mixture fraction	0.27
Co-flow velocity	0.9 m/s

In a more recent paper, Garmory and Mastorakos [17] performed large eddy simulations with a CMC model and discussed sensitivity to mesh size and boundary conditions during extinction/reignition. In [18], Ferraris and Wen used a large eddy simulation-CMC model with conditional quantities expressed as an expansion in steady flamelets. Reasonable prediction of unconditioned source terms were reported for the D flame but the model is unable to predict the transient phenomenon of local extinction/re-ignition due to the use of steady flamelets. These methods all use large eddy simulations for the flow calculations rather than the simpler RANS equations applied in this work. As is common in large eddy simulations the conditioned quantities are transported on a separate coarser grid, a simplification not made in this thesis. Ihme and Pitsch [19] apply a large eddy simulation model with a simplified conditioning of a progress variable and use a presumed PDF for that progress variable.

Brizuela, [20], presented a RANS simulation of the Sandia D flame using a CMC model with a similar setup as in this thesis. A 4960 cell 2-dimensional mesh, a small 16 species mechanism and 69 mixture fraction grid points were used. Different distribution functions for conditional scalar dissipation and the mixture fraction PDF were discussed and results are reported to improve when these distributions are consistent.

2.8.2 LTIF-CMC

The LTIF-CMC model applied in this work is based on the CMC approach with progress variable and tabulated transient flamelets. Conditional reaction progress is transported on the same grid as all other field variables. This method has mainly been applied to in-cylinder combustion for engine simulations and for burning sprays and is described by Lehtiniemi, Borg and Mauss in

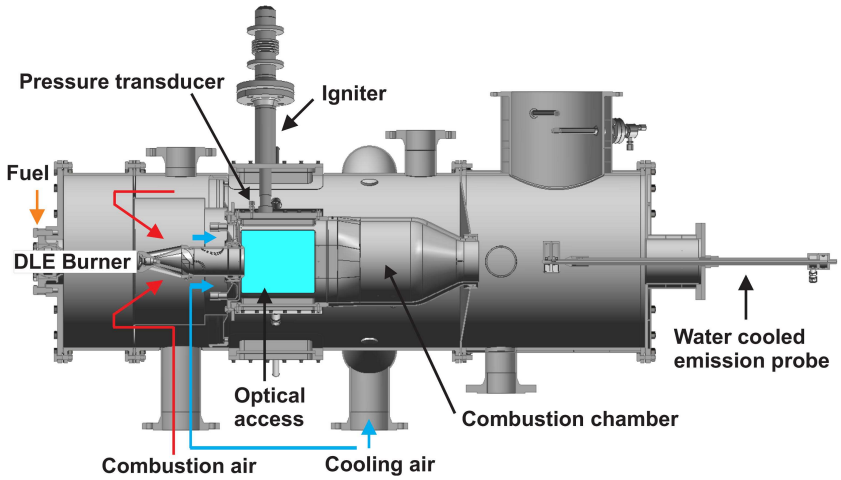

Figure 3: The atmospheric combustion rig at Siemens Industrial Turbomachinery (SIT) [2].

[7]. It is a natural step to evaluate the performance of the model for turbulent jet flames.

2.8.3 Siemens Burner Rig

Several models and experimental methods have been applied to the Siemens burner rig including computational fluid dynamics with both RANS and large eddy simulations, simple reactor networks and laser based measurements. Some examples are the publications by Lörstad et al. [21], Lörstad et al. [22] and Lantz et al. [2] concerning both experimental and simulation studies and the theses by Bruneflod [23], Hamedi [24], Marashi [25] and Bosyi [26]. In [14] by Lörstad et al. the burner system and fuel capability is described and an increase in allowed fuel hydrogen content from 10 % to 15 % starting from year 2013 is announced.

2.8.4 Reactor Network

There are several examples of reactor network models in the literature, mostly based on homogeneous reactors. Various methods to construct these networks have been applied. Fichet [27] and Falcitelli [28] have suggested construction methods based on splitting selected variables into series of intervals. In the method described in [28] splits of several key variables is first performed followed by a check for geometrical connectivity within the formed zones. This results in a large number of zones. Then only the N zones with the biggest number of cells are kept and all cells from smaller zones are redistributed over the remaining zones. The zone to place a redistributed cell in is selected by minimizing the increase in the zones' "unmixedness index", which is essentially the sum of the variances in selected variables. This method can produce a predefined number of zones, it can take arbitrary variables into account and good results have been reported. A possible drawback of this kind of method is that some of the small zones (few cells) may represent important parts of the domain not suitable for redistribution of cells. There is also no limit to how unmixed a zone may become during the redistribution process. The method reported in [28] is the most similar method to what is applied in this thesis.

The method by Fichet [27] is also based on series of intervals but an interesting feature is the introduction of a new transported field variable, a, called the "fluid age", which is defined through its source term $\frac{da}{dt} = 1$. The fluid age describes how long the fluid has been in the domain and can be useful when splitting recirculating flows. Some other examples of reactor networks for gas turbine conditions include the works by Marashi [25] where small, manually

constructed reactor networks are used to study a Siemens SGT-700 combustor, and Drennan [29] where a filter-based method is used to generate reactor networks for gas turbine combustion.

In [26], Bosyi uses networks of homogeneous reactors to simulate Sandia flame D and the Siemens burner rig. To construct those networks Bosyi used the same computational fluid dynamics results that were computed within this thesis. Small networks (order of 10 zones) constructed based on temperature and geometric connectivity were applied. Such networks are reported to give reasonable results and predict the right trend in nitric oxides for increasing hydrogen content in the fuel. The necessity of taking parameters like temperature into account when building the network is pointed out.

The construction method suggested in this thesis differs from [28] and most other methods in that it performs the splitting not in each physical variable separately but instead in linear combinations of (normalized) physical variables. This allows for correlations between variables to be taken into account during the construction. A full description of the construction method is given in section 3.2.

3 Model Development

In this chapter the new development done in this work is described.

3.1 Extension of Pre-existing CMC Code

In this work a pre-existing CMC code [7] was extended for jet flame simulations. This included the treatment of open boundary surfaces which are used for inlets and outlets. A method to ignite a pre-calculated cold flow was also implemented. In this method an unburned progress variable profile is initiated and then slowly changed into a burned profile in a small part of the domain during the course of the flow calculation. This ignition process avoids the occurrence of sharp artificial gradients that may cause numerical instabilities.

3.2 Reactor Networks

In the second part of this thesis, two methods are developed by which reactor networks can be constructed from a computational fluid dynamics (CFD) simulation. These methods are also applied to both the Siemens burner rig and the Sandia D flame. For the reactor network, computational grids are split into a number of larger connected zones. No flow computation is performed in the network, instead, the flow is derived from a pre-calculated computational fluid dynamics solution. This means that the network method relies on the assumption that the flow field calculation has been accurate enough, which in turn requires accurate chemical heat release and thermodynamics in the computational fluid dynamics simulation. This is tested in this thesis by performing two computational fluid dynamics simulations, one with a simplified chemical scheme and one with a more detailed chemical scheme.

The motivation for having a network model is to decrease computational time by separating the computation of flow and major combustion reactions from the calculation of detailed minor-species chemistry. First running a flow simulation with a simple combustion model to get the flow field and then computing detailed chemical information, such as nitric oxide concentration, with a network model could give a shorter overall computational time than using advanced combustion models directly in computational fluid dynamics. Networks can also be used to extrapolate from a computational fluid dynamics simulation and study trends for moderately varying fuel composition and temperature.

The main goal of the network part of this thesis is to develop methods to automatically generate a network and map the flow field onto it in a way such that the most important regions get the finest discretization. This resulted in two different methods, one based on principal component analysis (PCA) and the other based on cluster growth. These methods are described in the sections 3.2.1 and 3.2.2.

The splitting of the flow field into a number of zones should be done by clustering cells to make the zones as homogeneous as possible. Preferably each zone should also be a geometrically connected cluster of cells in order to keep the flow between zones low. Before a method for such clustering can be constructed the meaning of "as homogeneous as possible" should be discussed. Each zone in the network is to be modeled by either a homogeneous or stochastic reactor. These reactors are described in more detail in sections 2.4 and 2.5, respectively. For a homogeneous reactor it is assumed that the gas mixture is homogeneous but for a stochastic reactor that assumption is relaxed a bit by just assuming that the mixture is statistically homogeneous and a realization of the PDF is represented by an ensemble of particles. What the assumption of statistical homogeneity means in practice is that each particle is equally likely to mix with any other particle within the reactor. Thus, the cells in a zone need not have the same chemical

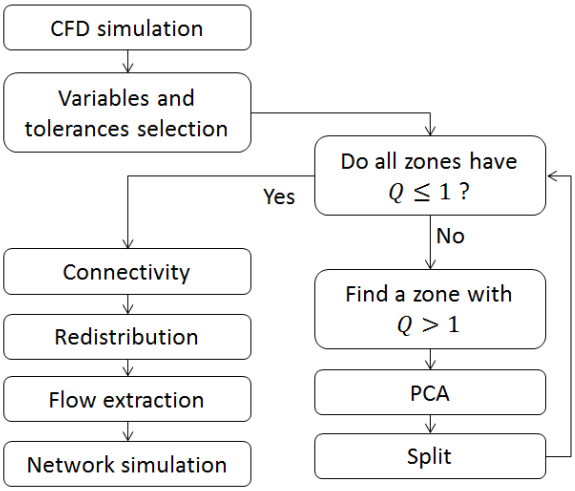

Figure 4: Flowchart illustrating the PCA-based method for construction of reactor networks.

composition, temperature or reaction progress but they should be geometrically and chemically close enough to justify statistical homogeneity.

3.2.1 Network Construction Using PCA

To perform the splitting into zones, a set of relevant field variables needs to be selected. These variables could be mixture fraction, species concentrations, reaction progress, velocity components, density, turbulent kinetic energy, eddy dissipation rate and temperature, but also the spatial coordinates x, y and z can be appropriate. Fichet [27] also suggests a special "fluid age" tracer, which is a field variable with a constant source term, to be used for example to detect recirculation zones. The use of spatial coordinates is mainly to help enforce geometrically compact zones.

Given a set of field variables it is proposed to create zones by minimizing variances within the zones. First, dimensionless versions of the selected variables are defined by normalizing them to zero mean and dividing them by reference values which serve as tolerances. The second step is the application of a principal component analysis (PCA) which finds the direction along which the variance of data points is maximized. The data points here are discrete volume elements (cells) so let $\boldsymbol{x}_i = (f_i^1, f_i^2, f_i^3, \dots)$ be a vector containing the normalized field variables $f^1 ... f^n$ of cell i and m_i be the mass of cell i. Then which is the direction of maximum variance is given by the eigenvector u corresponding to the largest eigenvalue of the covariance matrix

$$R = \frac{1}{N} \sum_{i=1}^{N} m_i \boldsymbol{x}_i \boldsymbol{x}_i^T \tag{35}$$

where N is the number of cells in the set. A split location is selected along the direction defined by this eigenvector such that the sum of variances for the resulting zones is minimized. To do this, the coordinates $c_i = u \cdot x_i$ in this direction are computed and sorted, all $N - 1$ splitting possibilities are tested and the one which gives the smallest summed variance is selected. The method is then repeatedly applied to the resulting zones until all zones have a "zone quality" $Q < 1.0$ (less is better). The zone quality could for example be the standard deviation in the first principal component in the zone or one of other measures about to be described. A flowchart is shown in Figure 4 that illustrate the PCA method.

There is a drawback with the use of standard deviation as indicator of zone quality that needs to be discussed. The problem is that a zone with many cells may have a small variance even if there are a few extreme outlier cells in the zone. Consider for example a zone in the Sandia D flame defined to include the lower part of the main fuel inlet an the entire co-flow. Clustering is done on temperature and mixture fraction. This zone has a very low variance since all cells are close to 293 K and the fuel inlet cells with mixture fraction 1.0 are so few (and small) that they do not contribute much to the variance. No further splitting is done on that zone unless the tolerances are very small (exactly this kind of zone has been observed). Scanning for geometric connectivity only partially solves this problem since there may still be a small number of highly deviating cells in a connected zone. One solution would be to use intervals rather than variances as zone quality. The interval of a zone could be defined as

$$I = \max_{i,j} |\boldsymbol{x}_i - \boldsymbol{x}_j| \tag{36}$$

which is the distance between the two points furthest away from each other (the diameter of the set). The corresponding zone quality would then be $Q = I/2$. Using intervals as stopping criterion gives an inconsistency when the direction along which to split a zone is based on minimizing variance: the splitting procedure is not trying to fulfil the actual stopping criterion. If (36) is used it makes more sense to split along the direction defined by $\boldsymbol{x}_i - \boldsymbol{x}_j$ to quicker fulfil the stopping criterion. Finding this direction (the indexes i and j) is no easy task because the number of distances that has to be calculated and compared scales as n^2.

Alternative zone quality measures that are easier to calculate include the interval in the principal component direction or the maximum interval over all directions that represent the pure cluster variables. The latter is used in this thesis and can be expressed as

$$Q = \frac{1}{2} \max_q (\max_i x_{i,q} - \min_i x_{i,q})$$

where i runs over all cells in the zone and q runs over all variables. Splitting is done in the principal component direction despite the inconsistency outlined above. The motivation for this choice is to avoid the variance problem described above and that it is easier to estimate the effect that a change in some tolerance will have on the splitting when using an interval-based zone quality.

The splitting procedure outlined above easily results in geometrically disconnected zones so further splitting of disconnected zones is needed. This extra splitting based on connectivity usually results in many small zones (containing only one or two cells) that will mainly just slow down the network simulation, therefore it was decided to take all zones with less than a certain number of cells and redistribute their cells to other zones. What zone a cell is moved to is decided by the requirement of connectivity and the smallest violation of the stopping criterion.

The amount of mass flowing between zones is extracted from the computational fluid dynamics flow field using the net flow for each connected cell-face pair.

3.2.2 Network Construction Using Cluster Growth

In this section a method based on cluster growth is described. This method is only briefly tested in this work. The same normalized field variables and stopping criteria as in the PCA based method are used. The difference is that the cluster growth method does not start out with the whole domain as one big zone and the task of dividing it. Instead, this method starts from a single cell and forms a cluster by adding neighbouring cells to build up a zone. The cluster growth stops when there are no more neighbour cells that can be added without causing $Q > 1$;

when this happens a new cluster is started from a cell selected among the ones not already classified.

The advantages of this method is that the zones fulfil both tolerances and connectivity without requiring a separate connectivity check and it is slightly more efficient since it does not have to search for any optimal split location. A possible drawback is that the network will depend slightly on the order in which the cells are tested.

3.2.3 Homogeneous and Stochastic Reactor Networks

Both homogeneous and stochastic reactor networks have been used in this thesis. In this section we describe the reactor network simulations and the treatment of flow between reactors.

During a chemistry calculation the pressure is assumed constant. If constant volume would be assumed instead there would appear pressure differences between reactors and since the network does not solve a momentum equation such differences would never disappear resulting in non-physical solutions. Constant pressure, however, means that the gases are free to expand or contract and thereby change its volume which would no longer be equal to that of the cells the reactor represents. The solution to this problem used in this work is a third option where both pressure and volume are kept constant but the mass is allowed to vary. A constant pressure chemistry step is followed by a reset of the volume to what it was before, effectively changing the mass to $m_{new} = \rho_{new}/V$. For a homogeneous reactor, this is practically done by recalculating the residence time using the new density and the old volume. Resetting volumes does not conserve mass but this is not an issue since a steady state is sought which, when all densities have converged, does conserve mass.

The stochastic reactor network has the flow completely separated from the chemistry giving a stronger dependency on time step size compared to a homogeneous reactor. Because the flow is done in one step, outflow followed by inflow, the time step must also be small enough that all mass is not removed from any reactor as outflow. Particle velocities are not tracked so during outflow particles are selected at random. At the domain inlet particles are created with the target particle mass of the zone, m_{zone}/N_{zone} where m_{zone} and N_{zone} are the mass and desired number of particles in the zone, respectively. Zones can have different target particle mass; during inflow this is handled by splitting big particles and merging small ones to keep the number of particles in a zone close to constant.

Another situation that requires a comment is how mixing is handled when homogeneous reactors have inflow from more than one other reactor. The pressure of the receiving reactor is used and mixing is done under constant enthalpy. Again, since the momentum equation is not solved in the network the pressure cannot be allowed to change in any reactor, the correctness of mass flows and reactor pressures extracted from the computational fluid dynamics solution is part of the assumption of the network.

3.2.4 Convergence Criteria

For a homogeneous reactor the steady state convergence criterion is that all mass fractions in all reactors must change less than a given tolerance during one time step. A stochastic reactor does never reach a true steady state due to the random mixing. Instead, mass fractions and temperature are averaged over a certain time and the steady state criterion is then applied to the temperature time average. The time interval over which the averages has to be calculated to be stable is not known a priori. Therefore the intervals are initially equal to the time step and then increased by 20 % each time a new average is calculated until the average has converged.

4 Results and Discussion

This section describes the setup of all simulations performed in this thesis followed by a discussion of the results. The computational fluid dynamics (CFD) part is discussed first and the reactor network part follows.

4.1 Flow and Chemistry Simulation Setup

All flow calculations in this thesis are done with the time dependent form of the RANS equations (also known as unsteady RANS or U-RANS). These transport equations are solved with a finite volume method in the computational fluid dynamics software STAR-CD [5]. The PISO (pressure implicit with splitting of operator) algorithm [5] and second order differencing schemes are used. The advantage of finite volume methods is that they conserve the primary variables in the flow equations and that complex geometries can be handled. Density is assumed to follow the ideal gas law, except for some cold flow simulations which were made incompressible for stability and to save time.

Several different chemical mechanisms have been applied in this work. The first mechanism is a 163 species scheme designed for natural gas combustion by Schenk [30], which will be refered to as the 163 species mechanism. This mechanism contains species with up to 7 carbon atoms and many of these species are short-lived radicals. There is nothing special about the number 163, it is just the number of species that turned out to be of relevance when the mechanism was developed. The second mechanism has 28 species and is a reduced skeletal version of the 163 species mechanism and has previously been applied by Marashi for reactor network modelling [25]. This mechanism does only contain species with up to 3 carbon atoms. Neither of these mechanisms contain nitric oxide chemistry so a modified version of the 163 species mechanism was created by adding extended Zeldovich thermal nitric oxide chemistry, giving a 166 species mechanism (the additional species being N, NO and NO_2). This modified mechanism was validated by comparing ignition delay times with the original mechanism.

For studying how NO formation is affected when hydrogen is added to the fuel in a reactor network it was required to include prompt nitric oxide formation in addition to the thermal provided by the extended Zeldovich reactions. Prompt nitric oxide formation is a collective name for reaction paths involving a direct reaction between N_2 and radicals from the combustion. Here, the 53 species GRI 3.0 mechanism [31] for natural gas was used, as well as a the 163 species mechanism with the nitric oxide part of the GRI mechanism added to it giving a 180 species mechanism.

Computation of chemistry (mass fractions in case of the homogeneous reactor model and progress variables in case of the LTIF-CMC model) is done with the chemical kinetics software LOGEsoft [32]. Flow and chemistry calculations are separated via operator splitting: the RANS equations are first solved in STAR-CD with the chemical source term $\overline{\omega_k}$ removed, then a mass fraction or progress variable update is made by solving the remaining parts of the appropriate equations once per time step by LOGEsoft.

4.2 Computational Fluid Dynamics Analysis of Sandia Flame D

For baseline cases Sandia flame D was calculated with both homogeneous reactor chemistry and CMC. One reason for doing the homogeneous reactor simulations was to motivate the use of more advanced models and to have a starting point for reactor network construction. Typical computational times for the flow simulations of the Sandia flame range from one to a few days on 12-20 cores depending on the chemical model.

4.2.1 Mesh and Boundary Conditions

The main inlet diameter of 7.2 mm was used as a reference and is referred to as D, see Table 2. Cylindrical symmetry was assumed and a 6° sector mesh consisting of a single cell layer was used. $5D$ length of burner pipe was included in the mesh.

The mesh has 10768 cells and is 10 cm wide ($14D$, 90 cells) and 55 cm high ($70D$, 120 cells) with smaller cells close to the main inlet, see Figure 5. Mesh sensitivity was not studied but the mesh is motivated by its resolution being comparable to what was used in RANS by Brizuela [20] and finer than the mesh used by Jangi [33] for transported PDF.

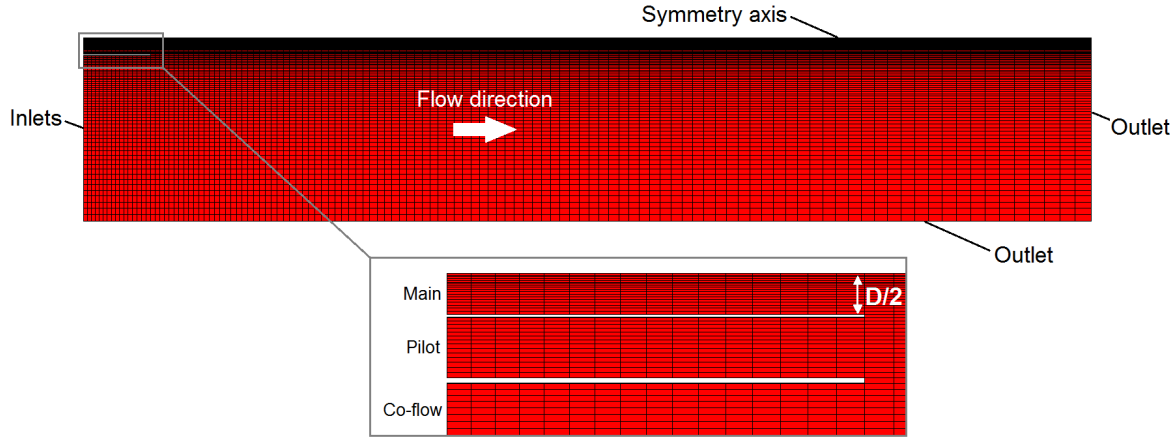

Figure 5: 2-dimensional mesh for Sandia flames. The smaller picture at the bottom is a close-up view of the inlets. The flow direction is from left to right.

Velocity profiles, temperatures and species compositions for all inlet boundaries were taken from the measurements described in [13]. Turbulent length scales were estimated as 10 % of the tube diameter at the main inlet, 50 % of the pilot inlet thickness for the pilot and 5 cm for the co-flow. Turbulence intensity 0.1 was used at all boundaries. Turbulence parameters at the boundaries are small compared to what is observed in the rest of the domain so these values should have insignificant effect on the solution.

Outer boundaries were defined as constant pressure surfaces with a temperature of 293 K; this temperature is only relevant in case of inflow. Periodic boundary conditions were used at the sides of the mesh and walls in the inlet tubes were modeled as adiabatic non-slip walls. Adiabatic means that the wall temperature is always equal to the temperature in the neighbouring cell so that there is no heat exchange between the wall and fluid and no-slip means that the velocity is zero at the wall surface.

For CMC simulations additional boundary and initial conditions are required for the conditional reaction progress. At the main inlet, co-flow inlet and as initial condition in the domain, the reaction progress is a linear function in mixture fraction space:

$$\langle h_{298}|Z=\eta\rangle = h_{298}(\eta=0) + Z \cdot h_{298}(\eta=1)$$

Here the end point $\eta = 0$ corresponds to pure oxidizer (co-flow) and $\eta = 1$ corresponds to the fuel mixture at main inlet conditions. For the pilot flame consisting of pre-burned gases, the conditional progress was set to a completely burned profile. It is pointed out that the progress at the fuel side, $h_{298}(\eta = 1)$, was treated as a constant even though reactions could theoretically occur in this mixture. This is done to simplify the boundary conditions for flamelets and practically means that reactions start at the second grid point. Mixture fraction variance $\widetilde{Z''^2}$ was set to zero at all inlets.

4.2.2 Homogeneous Reactor Simulations

Homogeneous reactor simulations have been performed for Sandia flame D. The baseline case uses the 163 species chemical mechanism, the k-ε turbulence model (described in section 2.2) and all the specifications above. The effect of the choice of turbulence model was briefly studied by running the same simulation with a Reynolds stress model instead of k-ε. A comparison between the 163 and 28 species mechanisms was made to make sure that the reduced mechanism is applicable to this problem. These simulations all made use of a clustering method that lumps together cells that differ less than 2.5 % in mixture fraction and enthalpy of formation during chemistry computation to speed up calculations. To make sure this does not affect the results, the baseline case was also run without clustering.

It was observed that the flame would not ignite from just the heat provided by the pilot if a transient simulation was started with the specified boundary conditions and initial conditions corresponding to air standing still. It was found that a reliable way of getting an ignited flame is to first decrease the inlet velocity to about one third and make a cold flow calculation (chemical reactions turned of). Then chemical reactions are turned on, the heat from the pilot ignites the flame and the inlet velocity can then be increased to the appropriate value. Once a fully developed flame has been achieved the simulation is run for about 3 flame flow-through times to make sure a steady solution has been reached. An estimate of the flow-through time was obtained by following massless particles from the inlets until they reach the top of the mesh. The longest time from the pilot inlet was about 0.04 s.

4.2.3 CMC Simulations

Sandia Flame D was computed using the same baseline setup as in the homogeneous reactor case. A flamelet table was made for this calculation using the 166 species mechanism, five different scalar dissipation rates ranging from 0.05 to 1000. A mixture fraction grid containing 104 points (including the boundaries) was used. In simulations of Sandia flame D the grid was reduced to 73 points with higher density below $Z = 0.45$, see Figure 6. The reduction was done since using all the 104 point present in the table made the simulations considerably slower.

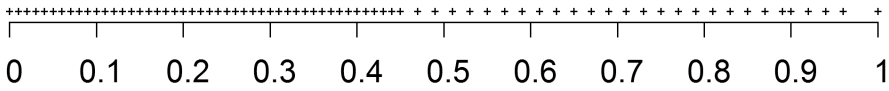

Figure 6: Mixture fraction grid used in CMC simulations of Sandia flame D.

4.2.4 Results

Experimental data for the Sandia flames, [13], are available along the axial centre line and radially at heights 1, 2, 3, 7.5, 15, 30, 45, 60 and 75 D, where $D = 7.2$ mm is the diameter of the main inlet.

All spatially resolved results with homogeneous reactor chemistry were averaged over 0.01 s with 50 points unless otherwise stated, which is based on periodicities of approximately 0.003 s observed in the flame. The effect of time-averaging the mixture fraction field is only important just above the pilot inlet as is apparent from Figure 7 where the root-mean-square (RMS) deviation from the time average is plotted for the homogeneous reactor baseline case. Maximum RMS deviation was found to be about 0.06. Temperature profiles of the homogeneous reactor baseline and CMC are shown in Figure 8, illustrating the shape of the flame. It is seen that

the CMC model predicts a lift-off, meaning that the flame is detached from the burner outlet. There should not be a lift-off in this flame, this problem will be further discussed later.

Figure 7: Root mean square (RMS) fluctuations from time averaged mixture fraction over 0.01 s. Calculated for the Sandia D homogeneous reactor 163 species baseline case.

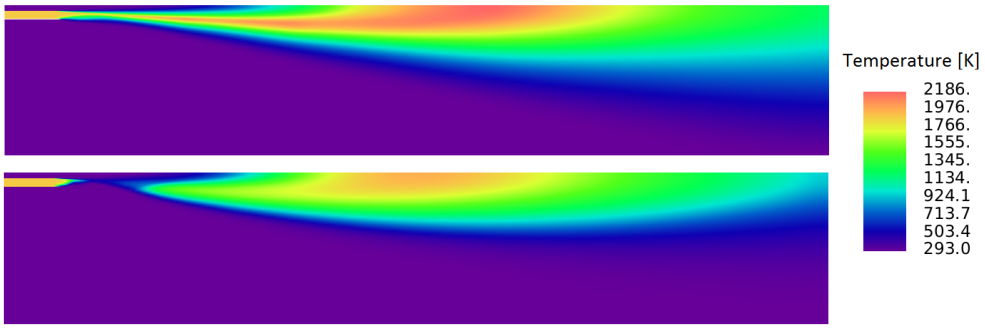

Figure 8: Temperature [K] of the D-flame simulated with homogeneous reactor chemistry (top) and CMC (bottom) using the 163 and 166 species mechanisms, respectively. The flow direction is from left to right.

Mixture fraction profiles were computed using the scalar transport equation (22) and appropriate boundary conditions from Table 2. These profiles are compared to experimental data along the flame axis (center line) and along radial lines at heights 15, 30 and 45 D in Figure 9. It is seen that mixture fraction is too low along major parts of the centre line. Radial profiles at 15 and 30 D reveal that mixture fraction is too high further out from the axis, indicating too rapid turbulent diffusion. In the CMC, high mixture fractions moves outwards to an even larger extent as seen at height 15 D, part of this effect is likely due to the lack of heat release in the lift-off region.

Figure 10 shows mass fraction profiles for OH and formaldehyde and Figure 11 shows center line temperature for the baseline homogeneous reactor case with and without cell clustering and for the CMC. Overall, good agreement is seen between the homogeneous reactor case and the experimental data. The flame shape, as indicated by these profiles together with the mixture fraction field, is wide in the radial direction and axially compressed. It was concluded that the cell clustering does not have a large impact on the results. In CMC the OH and CH_2O fields are wider in the radial direction and the temperature is axially even more compressed, again the lift-off is a likely reason. Also, an envelope of half-burned fuel surrounding the flame is seen in the CMC; this is clearly seen around 70 D on the plot of the centre line in Figure 10. A similar envelope is present also in the homogeneous reactor simulation and in the experimental data but of much lower magnitude (not visible in the plots). The envelope separates from the main flame front just above the lift-off region in the CMC.

The prediction of peak values of both temperature and the OH concentration show considerable improvement in the CMC simulation compared to homogeneous reactors although the

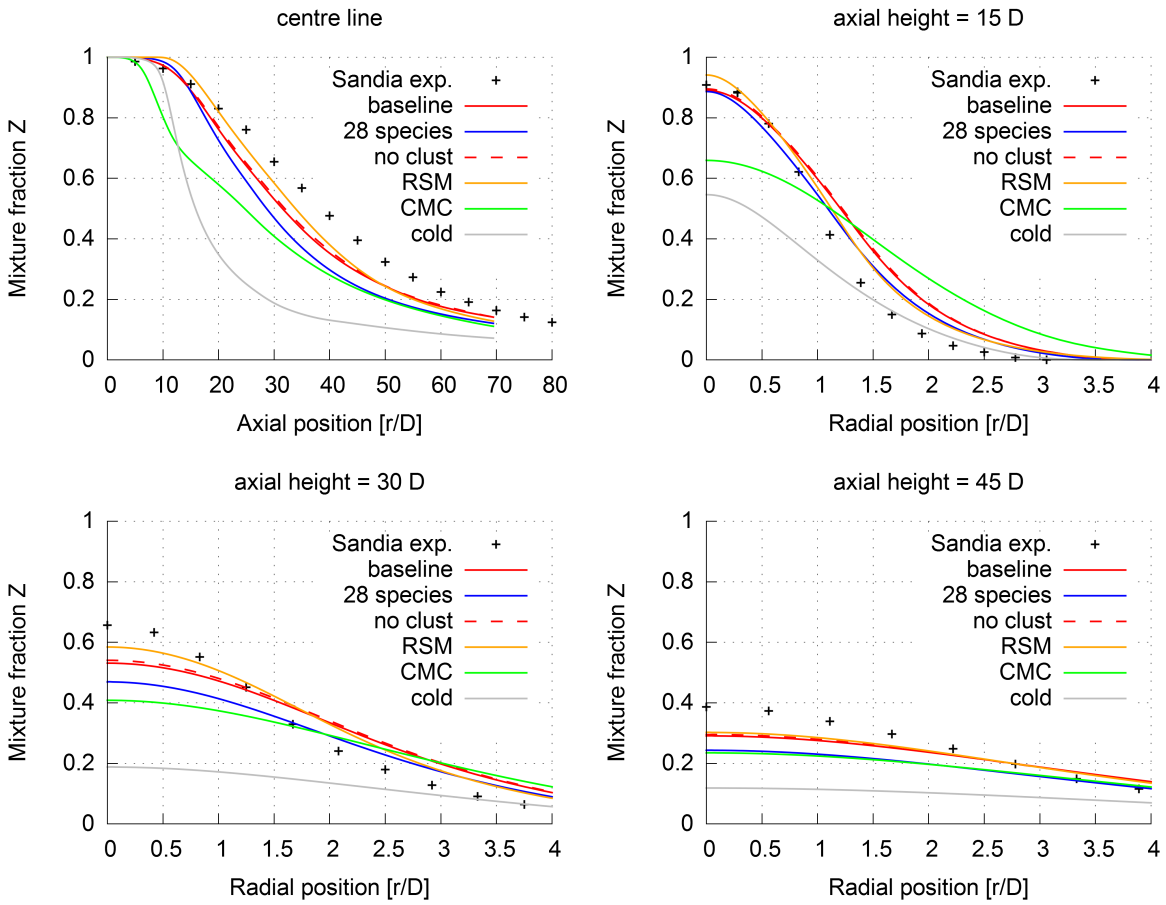

Figure 9: Sandia flame D calculated and experimental mixture fraction profiles along the centre line and radial profiles at heights 15, 30 and 45 D.

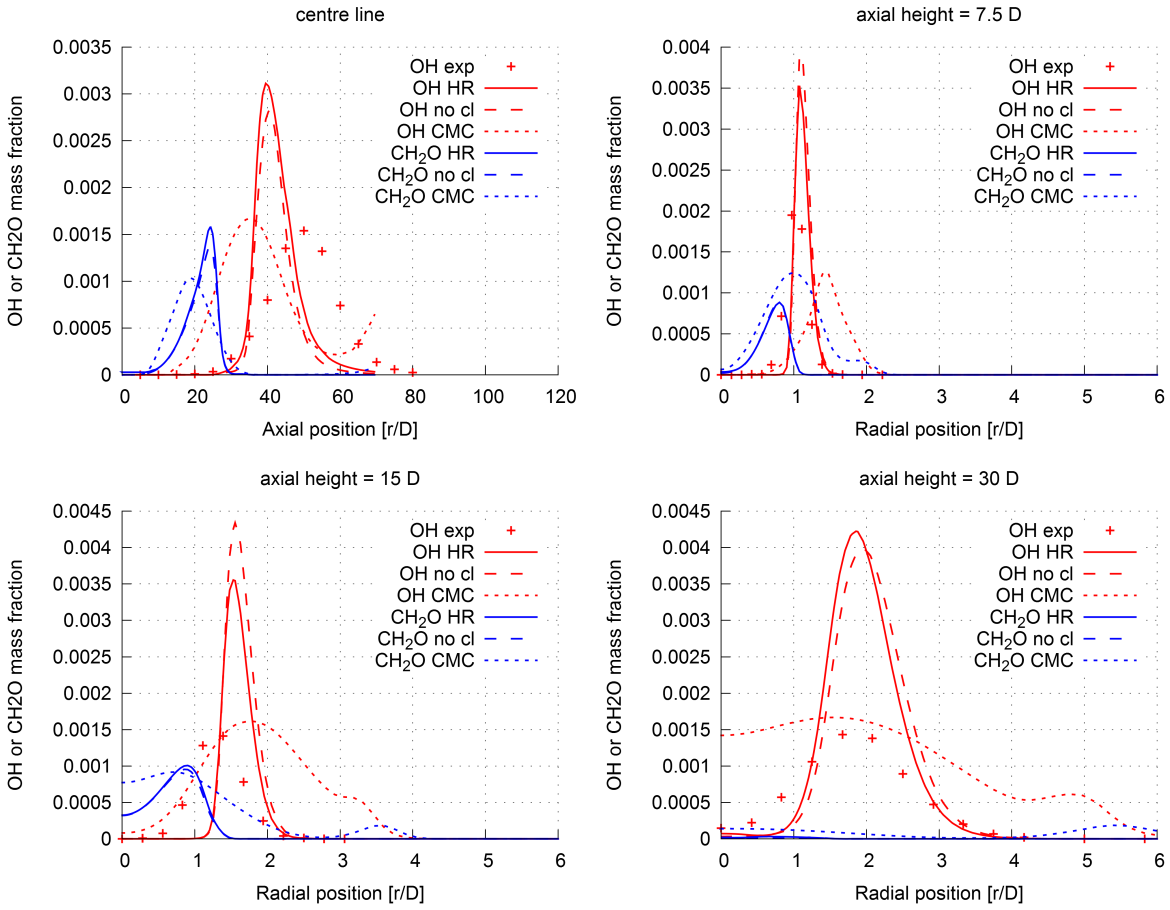

Figure 10: Sandia flame D OH and CH_2O mass fraction profiles along the centre line and radial profiles at heights 7.5, 15 and 30 D.

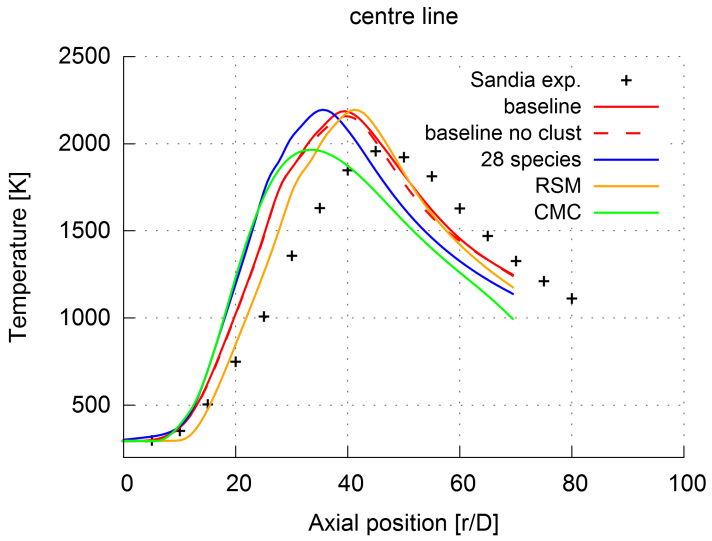

Figure 11: Sandia flame D center line calculated and experimental temperature.

spatial location of these peaks are more shifted due to the lift-off. The homogeneous reactors over-predict the peak values because of the assumption of perfectly mixed cells.

Not much difference is observed between the two turbulence models. The Reynolds stress model improves slightly over the k-ε model by making the flame a bit less compressed.

CO mass fractions conditioned on cell-average mixturre fraction predicted in the homogeneous reactor baseline simulation are shown in Figure 12. The plot depicts the CO mass fraction versus mixture fraction for each cell along a radial line at one instance of time. No time averaging has been made because both mixture fraction and CO vary with time and the averaged quantities may not have the same connection to each other as the instantaneous values do, the same effect that is described by equation (24). Only the average mixture fraction value per cell is available in the homogeneous reactor simulation since no sub-grid information is solved for. This is not the case for combustion models such as CMC or transported PDF. The bars show RMS deviations indicating the spread of experimental data points.

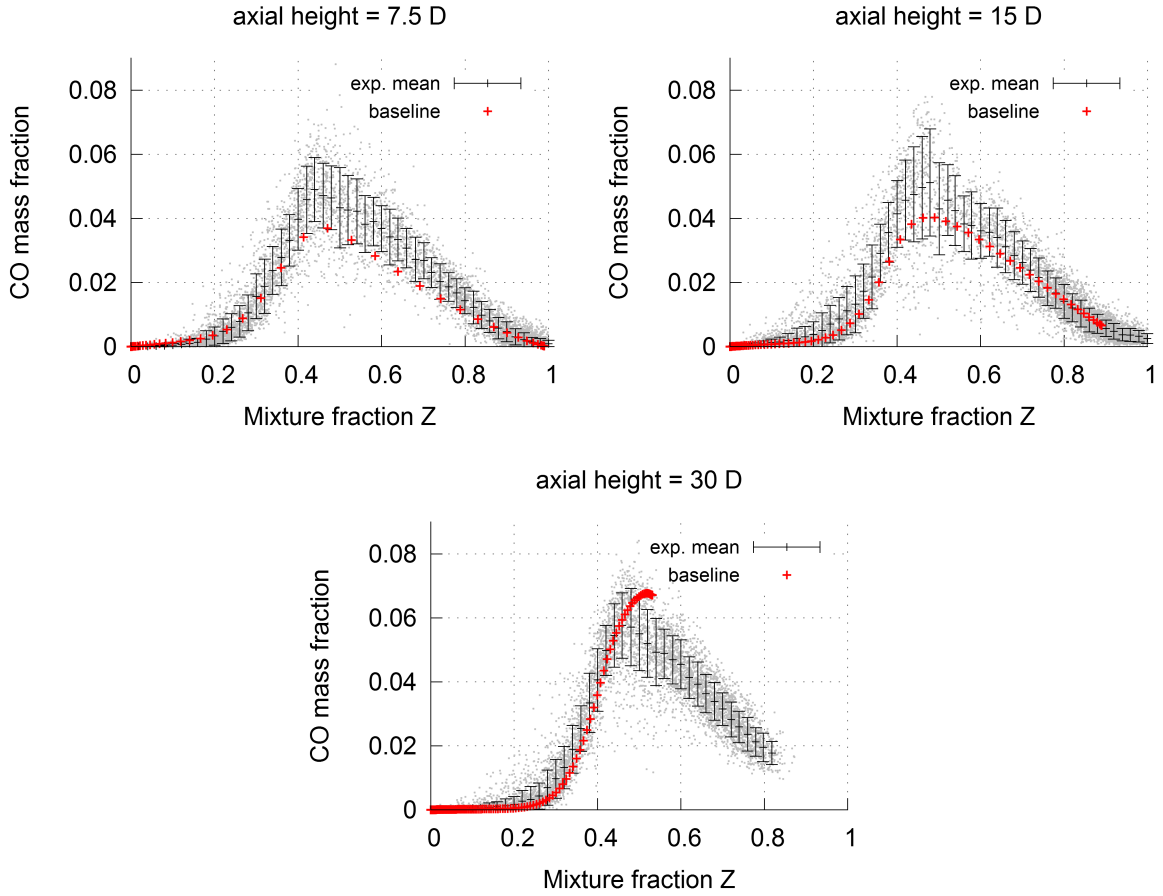

Figure 12: Sandia flame D conditional CO mass fraction at heights 7.5, 15 and 30 D for baseline 163 species homogeneous reactor simulation. The bars indicate RMS spread of experimental data and the small dots are individual measurements.

With the CMC model a lift-off of a few D is predicted which is not seen in either experimental data or the homogeneous reactor simulation. Mixture fraction and other field variables show bigger errors downstream but this may be a result of the lift-off. Maximum temperature is better predicted than with homogeneous reactors but seen in the wrong location as seen in Figure 8. In [34], Barlow presents measurements of scalar dissipation rate and mixture fraction variance at selected heights. Comparing to that, the calculated scalar dissipation at $h = 2D$

(the most upstream part of the lift-off region) is of the right magnitude but calculated variance in this region is too high. This may be an effect of the turbulence model or the mesh resolution around the walls separating the inlets. Too high a variance can lead to over representation of rich and lean states in mixture fraction space which are more difficult to ignite and easier to extinguish. If variance is the cause of the lift-off then that would also explain why no lift-off is not seen with homogeneous reactor chemistry since that model assumes perfect sub-grid mixing and is thus independent of variance in mixture fraction.

4.3 Computational Fluid Dynamics Analysis of Siemens Burner Rig

The procedure of the Siemens burner rig simulations was as follows: A cold flow was first calculated; a smooth ignition process was carried out and the simulation was run for two flow-through times to get a converged flow.

Because the system is premixed the mixture fraction grid resolution for the CMC calculations was reduced from the 104 points used in the table generation down to 13 points. Resolution is only needed close to the mean mixture fraction for this premixed system so this simplification was done to decrease computational costs. Typical computational times for flow simulations of the Siemens burner rig range from one to a few days on 12 cores.

4.3.1 Mesh and Boundary Conditions

Computations on the burner were performed using a 2-dimensional mesh provided by Daniel Lörstad at Siemens, see Figure 13. This mesh does not include the mixing chamber and swirl cone upstream of the burner; instead the velocity and turbulence profiles used at the inlet were taken from previous 3D calculations preformed by Bruneflod [23], which included these features. The chemical composition and temperature at the inlet are computed based on reported mass flow rates of fuel and air into the mixing chamber. Homogeneous reactor simulations used the 28 and 166 species mechanisms while CMC simulations used only the 166 species mechanism. Walls were either adiabatic or had constant temperature. For turbulence the k-ε model was used.

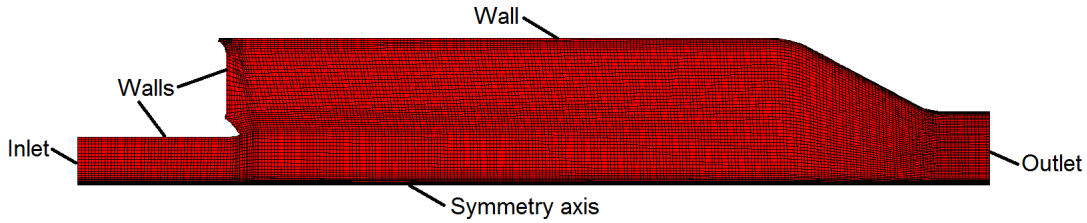

Figure 13: 2-dimensional mesh used in computational fluid dynamics simulations of the Siemens burner rig. This picture has been stretched for confidentiality reasons.

4.3.2 Oscillation Problem

Just like with the Sandia D flame, the rig simulations showed complications during start-up and ignition that had to be solved. The problem here is of a different kind and related to boundary conditions. Specifying an inlet velocity profile that is fixed in time is the main problem. While such a profile is expected to give a stable flow in the final steady state it was seen that enforcing the velocity profile from the start of a simulation lead to an unstable, heavily oscillating flow. If a fixed velocity is specified at a boundary then the density and pressure have to follow the values in nearby cells, which affects the influx of mass. The observed result is that the simulation

easily gets trapped in a state of oscillating density and pressure at the inlet and a velocity field that does not reach a steady state. A possible reason for oscillations can be that at the start of the simulation the velocity is zero everywhere except at the inlet boundary, giving some local compression of the fluid. A solution to this is to instead enforce a fixed mass influx profile and let the velocity vary accordingly. This reduces fluctuations in density and stabilizes the flow.

The method finally used for the cold flow was first to calculate an incompressible flow (which is stable with a fixed inlet velocity profile due to constant density) and then change to compressible flow with fixed inlet mass flux.

A problem with using a fixed mass flux profile at the inlet is that it requires knowledge of the inlet density profile in addition to velocity. Using a spatially constant density (estimated using the inlet temperature and assuming atmospheric pressure) for the entire inlet gave up to 10 % error in the velocity profile. It was however observed that once a steady cold flow had been reached it was possible to change the boundary condition to a fixed velocity profile and the flow remained stable as long as there was no combustion going on. Such a cold flow was calculated once and an inlet density profile was extracted and used for all further calculations. Figure 14 shows a validation of the resulting velocity profile.

It was also observed that the oscillations related to the use of fixed velocity inlet boundary conditions could be reduced if ignition is performed in a "smooth" way. Igniting with an artificial spark, for example by increasing temperature or burning to equilibrium in a few cells, creates a pressure wave which bounces back and forth in the domain causing more oscillations as it hits the inlet. If ignition is instead done by selecting some cells downstream of the expected flame front and slowly moving them towards chemical equilibrium at a fixed rate with spontaneous chemical reactions still turned off the temperature rises in a smooth and controlled way allowing pressure gradients to even out. Once the downstream zone is equilibrated the combustion model is turned on and a flame front forms in the boundary region between hot burned and cold unburned gases. This method does not introduce sharp pressure gradients and was observed to reduce oscillations when fixed velocity inlet boundary conditions were used and the method was applied throughout this work. It was later discovered, however, that the use of mass flow inlet boundary conditions alone are enough to avoid oscillations making the smooth ignition method unnecessary.

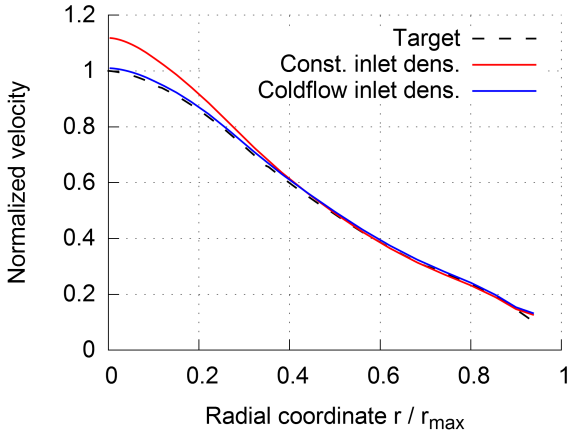

Figure 14: Inlet velocity profiles for Siemens burner rig calculated using a constant inlet density profile and an inlet density profile extracted from a cold flow calculation. Velocities are divided by the maximum value of the target curve.

4.3.3 Results

Velocity fields for the axial, radial and tangential (swirl) directions are shown in Figure 15. The velocity data is from the homogeneous reactor calculation with the 166 species mechanism but there is not much difference between the different cases, the plots are just to illustrate the general features of the flow. Temperature fields showing the flame shape is shown in Figure 16 for simulations with homogeneous reactor chemistry using the 28 and 166 species mechanisms as well as CMC using the 166 species mechanism. The NO fields are shown in Figure 17 for two different wall boundary conditions: adiabatic and fixed temperature. In Table 5 the outlet CO and NO mass fractions and the maximum flame temperature are summarized as well as corresponding results for the baseline reactor network. The computational fluid dynamics simulations were run transient and stopped when NO field did no longer change. Experimental NO values also include NO_2, which is not included in the calculated values but it is about 3 orders of magnitude less than NO.

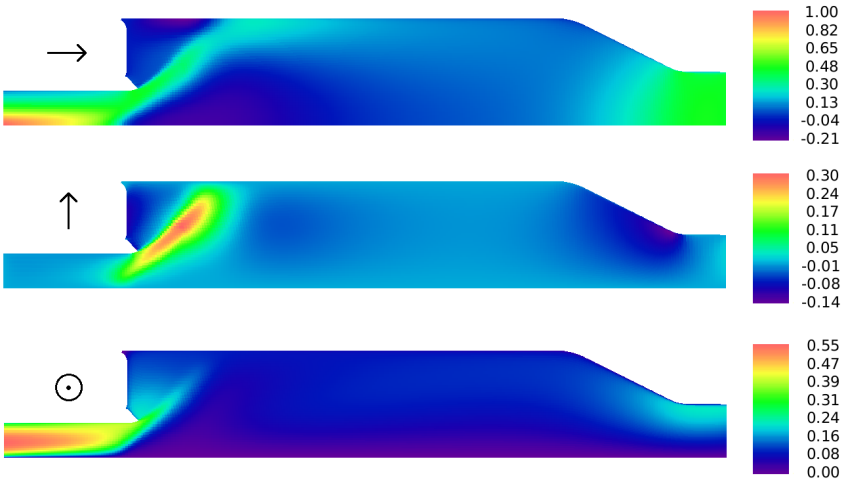

Figure 15: Axial (above), radial (middle) and tangential (below) velocity fields for the Siemens burner rig calculated with the 166 species homogeneous reactor model. The arrows indicate the direction corresponding to positive velocity. For confidentiality reasons the plot is stretched and a relative scale is used where all velocities are compared to the maximum velocity at the inlet in the axial direction.

Figure 16: Calculated temperature fields in the Siemens burner rig. For confidentiality reasons the plot is stretched and a relative scale is used where all values are compared to the maximum temperature in the 166 species homogeneous reactor simulation. Above: homogeneous reactors using the 28 species mechanism. Middle: homogeneous reactors using the 166 species mechanism. Bottom: CMC using the 166 species mechanism.

Figure 17: NO mass fraction fields in the Siemens burner rig calculated with the 166 species homogeneous reactor model. Above with adiabatic walls and below with fixed temperature walls. For confidentiality reasons the plot is stretched and a relative scale is used where all values are compared to the value at the outlet from the simulation with adiabatic walls.

Table 3: Outlet temperature and outlet NO mole fraction for computational fluid dynamics simulations with adiabatic and fixed temperature walls using the 166 species mechanism and for two experimental measurements.

Case	Cells	NO/NO_{ref}	T_{out}/T_{ref}
CFD adiabatic	15766	1.000	1.000
CFD fixed wall temperature	15766	0.650	0.956
Experiment 1	-	2.060	-
Experiment 2	-	1.762	1.026

It should be pointed out that the progress variable used in CMC in this work has not been selected with the intention of capturing minor species like NO in the post flame. Enthalpy of formation is hardly affected at all by slow NO reactions since these do not contribute any sizeable heat release. Thus the last entry in the flamelet library corresponding to a fully evolved flamelet may not have converged values for these species. This problem can be solved by storing NO source terms in the table instead of concentration and calculate NO separately during the flow simulation or by defining a progress variable that includes NO concentration.

Temperature and NO results are summarized in Table 3 for computational fluid dynamics simulations using the 166 species mechanism. The adiabatic walls give a 54 % increase in NO concentration at the outlet due to the lack of cooling. Compared to two independent experimental measurements the calculated outlet NO, with fixed wall temperature, are at 34 % and 39 % of the experimental values, respectively. It is seen in Figure 17 that NO formation stoops just after the flame front when the walls are cooled while it continues to be formed all the way to the outlet in case of adiabatic walls. This indicate that wall cooling is important for NO formation. The difference between the two experimental values is due to the measurements being made at two specimens of the same burner. These differences indicate that very small variations in e.g. geometry can be influence the performance of the burners.

4.4 Reactor Network Analysis of Siemens Burner Rig

Network analyses were performed both for Sandia flame D and the Siemens burner rig, but as it turned out that the Siemens burner rig is easier to calculate with a reactor network than the Sandia D flame main focus has been on the rig. The results are overall promising but there is room for improvement, especially for non-recirculating flows.

The computational times for the reactor networks used in this thesis range from one minute to around 40 hours on a single core. Stochastic reactor networks take the longest because every particle requires as much time as one homogeneous reactor. Small chemical mechanisms are

considerably faster because the chemistry calculation scales roughly as the square of the number of species. The big difference compared to the computational fluid dynamics simulations is that no flow is solved. It should also be noted that the computational fluid dynamics simulations done in this thesis use a clustering method that lumps similar cells together and gives a speed-up of at least a factor of 2 so a direct comparison of computational times with the reactor networks would be misleading.

4.4.1 Network Construction

A baseline reactor network was constructed for the Siemens burner rig using the PCA-based algorithm and the tolerances given in Table 4. These variables were chosen because they vary in different parts of the flame. The tolerances were decided by first setting all tolerances high, lowering one at a time until the partitioning was affected and then doing a test simulation to make sure a reasonable baseline network had been achieved. The geometry of the baseline network is shown in Figure 18.

Table 4: Variables and tolerances used to construct the baseline reactor network for the Siemens burner rig with the PCA method.

Variable	Tolerance
x and y coordinates	40 mm
x-velocity	40 m/s
y-velocity	20 m/s
Temperature	120 K
Density	0.05 kg/m^3
CH_4 mass fraction	$2.0 \cdot 10^{-3}$
OH mass fraction	$5.0 \cdot 10^{-4}$
O_2 mass fraction	$3.0 \cdot 10^{-2}$
CO mass fraction	$1.0 \cdot 10^{-3}$
Minimum number of cells	3

Figure 18: Baseline reactor network for Siemens burner rig constructed with the PCA method from computational fluid dynamics simulations based on the 28 species mechanism. All cells belonging to the same zone have the same color. Some disconnected zones also have the same color, this does not mean that they are the same zone. Every zone is a geometrically connected set of cells.

The baseline network was based on the 28 species homogeneous reactor computational fluid dynamics simulation and has 148 reactors. The number of reactors turned out to be quite sensitive to the tolerances, which originates from the fact that the effect of geometric connectivity and merging of small zones is very sensitive to small changes in the initial partitioning. For example, in the generation of the baseline network, the field was first split into 114 zones by the PCA-based split algorithm. The requirement of geometric connectivity split these further into 501 zones. Merging all zones with 2 cells or less gives the final number of 148 zones. This sensitivity adds a large amount of unpredictability to the number of zones when tolerances are

changed; if tolerances are made stricter in steps, the number of zones will increase in the long run but may even decrease locally from one step to the next. Also, all variables are initially scaled by their tolerances so if all tolerances are changed by the same factor the principal directions will not change. Then, as tolerances are made stricter, the number of zones after the initial split will increase only when a zone passes the limit of requiring one more split. If tolerances however are changed in a more arbitrary manner, the number of zones shows a more chaotic behaviour since even a small change in the principal components can have large effects on geometric connectivity.

To find how many reactors or how strict tolerances are needed to get a good network, a series of networks were constructed using the baseline tolerances multiplied by a factor. These networks were simulated using the 28 species mechanism and CO concentration and temperature at the outlet were compared. Variables used for the PCA and their corresponding baseline tolerances are summarized in Table 4. It should be noted that both CO and temperature are included in this list. The time step size was set to 20 μs for homogeneous reactor networks. For stochastic reactor networks a shorter time step, 10 μs, was required because of the separation of inflow and outflow as pointed out in section 3.2.3. For homogeneous reactor networks the convergence criterion was that all mass fractions should have a relative change that is less than 10^{-4} in one time step. For stochastic reactor networks the convergence criterion was instead that temperature should not change more than 0.03 between two consecutive time averages as described in section 3.2.4.

4.4.2 Sensitivity to Construction Tolerances

Results of sensitivity to scaling tolerances show that the outlet temperature and CO are not very sensitive. The scaling factors that were applied to the tolerances ranged from 0.3 to 5.5. Compared to the network with tolerance scaling 0.3 (515 zones) all networks up to scaling 2.0 (108 zones) differ less than 1% and with scaling 3.0 (66 zones) the difference is 7% compared to the network with the strictest tolerances. Only the 7 zone network constructed with tolerance scaling 5.5 show a big deviation. Figure 19 show normalized calculated CO as function of tolerance scaling factor and the corresponding zone numbers. Outlet CO is insensitive since CO is consumed near the flame front and mostly constant in the post flame, making it independent of post flame resolution. For very low resolution networks however, the error increases considerably as also the flame front loses resolution. The error in outlet temperature made by the network compared to the computational fluid dynamics simulation hardly improves when scaling down the baseline tolerances.

A downstream shift of the flame front compared to the computational fluid dynamics simulation is consistently predicted by the network. A likely explanation for this error is that convective and turbulent transport are not separated when the mass flow rates between zones are extracted from the computational fluid dynamics simulation. Only the net flux is considered for each pair of cell faces and this lead to reduced upstream transport of species and enthalpy.

The outlet temperature difference between the finest (515 zones) and the coarsest (7 zones) networks is 0.1%. Outlet temperature is insensitive to the network resolution because the combustion is complete in terms of heat release and because adiabatic walls (no heat transfer) are used. Outlet temperature is thus not an interesting variable to look at on its own but its insensitivity is helpful when investigating the highly temperature-dependent NO formation chemistry.

To check the sensitivity of NO formation to network construction a study was made where only the tolerances for spatial coordinates were multiplied by a scaling factor and all other tolerances left at their baseline values. The baseline network was used as starting point (scaling

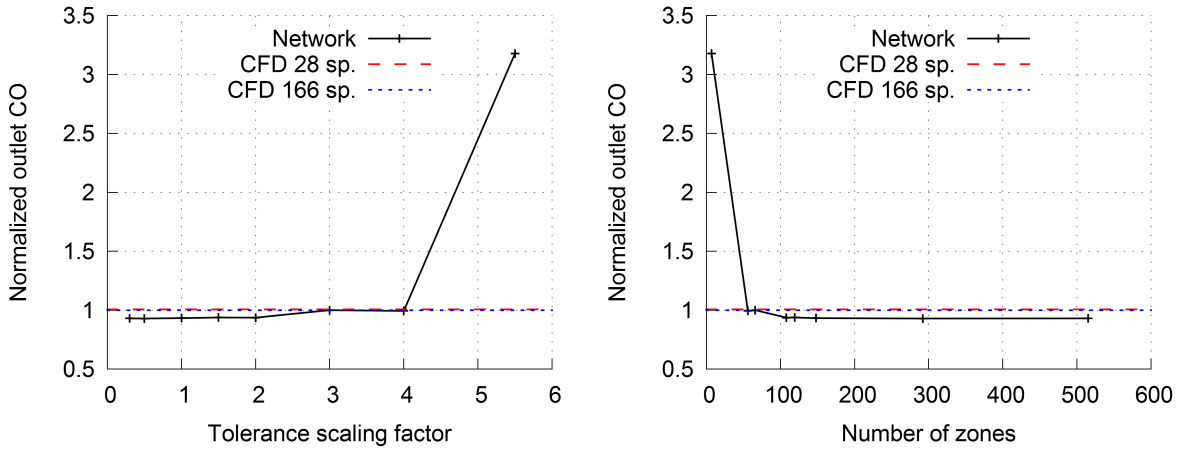

Figure 19: Outlet CO mass fraction in reactor networks for varying construction tolerances (left) and corresponding number of zones (right).

factor 1.0). Figure 20 shows the results of these calculations compared to the adiabatic 166 species computational fluid dynamics calculation. The results seem to converge toward the value seen in the computational fluid dynamics simulation.

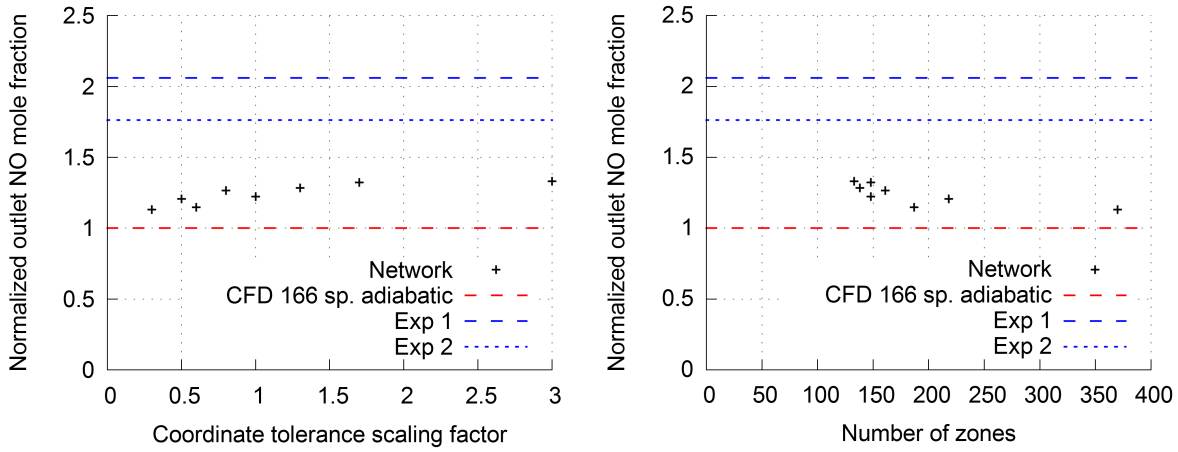

Figure 20: Outlet NO mass fraction in reactor networks for varying construction tolerances for spatial coordinates (left) and corresponding number of zones (right).

A network was also constructed with the cluster growth method and the baseline tolerances. This method was seen to give fewer zones compared to PCA with connectivity check. For the Siemens burner rig the cluster growth method was able to fulfil the baseline tolerances and connectivity (small zones allowed) using only 289 zones which should be compared to the 501 zones required by the PCA method. This means that with the cluster growth method it is not required to redistribute cells in small zones (and thereby violating the zone quality criteria) to achieve a small number of zones. No detailed investigation of the cluster growth method was made in this thesis.

4.4.3 Chemical Mechanisms

For comparison the baseline network was run also with the GRI 3.0 mechanism [31], which contain both prompt and thermal nitric oxide formation, as well as with the 163 species mechanism

Table 5: Outlet temperature, outlet CO mass fraction and outlet NO mole fraction for computational fluid dynamics and reactor network baseline cases with adiabatic walls. T_{ref} is for the computational fluid dynamics simulation with the 166 species mechanism.

Model	Reactors	Chemistry	CO/CO_{ref}	NO/NO_{ref}	T_{out}/T_{ref}
CFD	15766	28 sp	1.008	-	1.000
CFD	15766	166 sp	1.000	1.000	1.000
Baseline network	148	28 sp	0.933	-	0.997
Baseline network	148	166 sp	0.930	1.222	0.997
Baseline network	148	GRI	0.944	5.908	0.997
Baseline network	148	180 sp	0.930	4.390	0.997
Cluster growth network	289	166 sp	0.935	1.188	0.997
Experiment 1	-	-	-	2.060	-
Experiment 2	-	-	-	1.762	1.026

merged with the nitric oxide chemistry from GRI. Table 5 shows a five and four fold increase in NO, respectively. With GRI nitric oxide chemistry, N_2O makes up about 3 % of the total nitric oxides. This species is not included in the thermal nitric oxide chemistry used in the 166 species mechanism.

In Table 5 the baseline network is compared to computational fluid dynamics simulations with two different mechanisms. All these simulations had adiabatic walls meaning that there is no heat transfer to the walls.

4.4.4 Flame Temperature Effect on NO

The effect on outlet NO was investigated using the baseline reactor network with the 166 species mechanism which contains thermal nitric oxide chemistry. Different flame temperatures were obtained by varying the fuel/air ratio at the inlet. In the corresponding experiments only the inflow rate of fuel was varied but this has only a small effect on the overall mass flow rate since only 2-3 % of the mass is fuel. Calculated temperature and NO were both measured at the outlet.

Figure 21 shows normalized NO mass fractions as function of flame temperature on a log-scale because NO increases rapidly with temperature. The rate at which NO increases is over-predicted. The prediction for high temperatures improves slightly on what is reported [24] using computational fluid dynamics. A possible explanation for the over-prediction seen in Figure 21 is the use of adiabatic walls; it was seen in the computational fluid dynamics part (section 4.3.3) that heat transfer to the walls have a sizeable effect on NO formation.

4.4.5 Hydrogen Effect on NO

The effect of adding hydrogen to the fuel has been studied experimentally and in computational fluid dynamics by Lantz et al. [2]. In 2013 the allowed hydrogen content in the fuel was increased from 10 mol-% to 15 mol-% [14]. The reactor network based on the pure methane computational fluid dynamics simulation with the 28 species mechanism is now used in order to reproduce the observed trends and sensitivity of outlet NO when hydrogen is added to the fuel. Both in experiments and simulations the fuel inflow rate was adjusted to maintain a constant temperature over the range of hydrogen concentrations. It is reported in for example [2] and [22] that, in experiments and computational fluid dynamics with large eddy simulations, the whole flame front moves upstream with increasing hydrogen content. This may affect the flow pattern around the flame. This may limit how well the network can extrapolate from pure

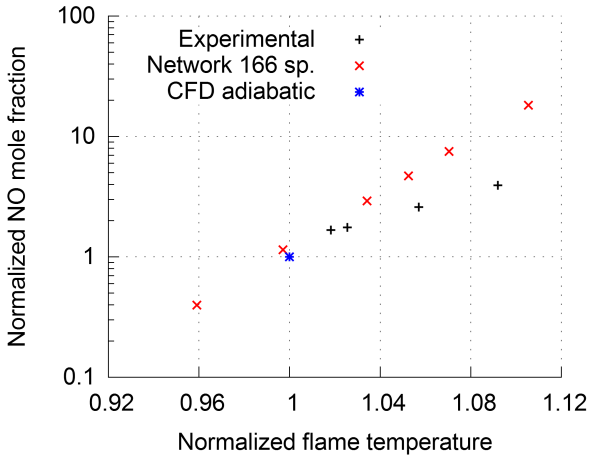

Figure 21: NO outlet mass fraction at varying flame temperature calculated with the baseline reactor network. The y-axis is in log-scale.

methane both because more error is introduced in the zone-to-zone flow but also because the network was constructed from a computational fluid dynamics simulation with a certain flame position and may therefore not have high resolution in the right places. If the chemical effects dominate, then the network may still be able reproduce the trend of NO formation.

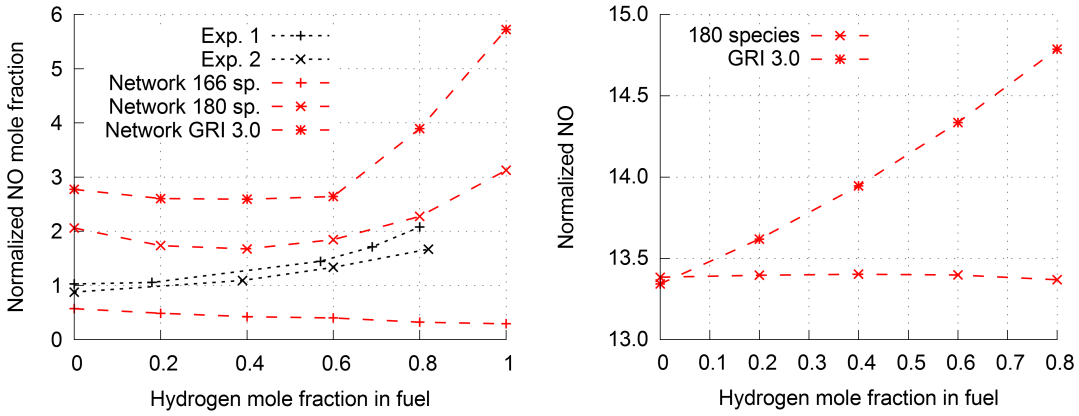

(a) **(b)**

Figure 22: (a) Normalized outlet NO in network simulations of Siemens burner rig using three different mechanisms. (b) Normalized NO in single homogeneous reactor calculation with the GRI 3.0 mechanism and the same volume as the rig.

Hydrogen concentrations used in experiments range from 0 to 82 mol-%. In the reactor network simulations six different concentrations, evenly distributed between 0 and 100 mol-%, were used. Figure 22a shows normalized outlet NO calculated with the baseline reactor network with homogeneous reactors and the 166 species, 180 species and GRI 3.0 mechanisms together with the results of two experiments. The experimental results are from two physically different burners (of the same type). Only considering chemical effects, varying hydrogen content is expected to change the NO level. This is because hydrogen affects the amount and types of radicals present in the flame. To predict these effects it is important to consider prompt nitric oxide formation, which is a result of reactions between nitrogen gas and radicals. In a burner also geometrical effects, such as flame shape and position, can affect the NO formation.

The 166 species mechanism does not include prompt nitric oxide chemistry, only thermal, and does therefore not predict any change in NO with increasing hydrogen. A slight decrease is even predicted which is a result of geometric effects. For the other mechanisms we do see a change in slope around 60 % hydrogen and an increasing NO concentration. A slight change in slope can be seen also in the experimental data but is clearly over-predicted by the simulation. In the 80 % and 100 % hydrogen network simulations the flame front makes a jump upstream in the simulations, almost into the burner, making the flame region smaller and the post-flame larger, which may have an effect on NO formation. This jump happens for all mechanisms and does not notably affect the case with only thermal nitric oxide chemistry, it may however be part of the reason that the other cases predict such a big change in slope. Upward movement of the flame is seen also in experiments and indicates a risk for flashback.

To isolate the effect of chemistry from the flow a single homogeneous reactor was also studied. The 180 species and GRI 3.0 mechanisms were compared for 0, 20, 40, 60 and 80 mol-% hydrogen. What is seen is that NO increases with hydrogen with the GRI mechanism but not in the 180 species mechanism indicating that the missing prompt nitric oxide chemistry in the latter is of importance. Figure 22b shows the result of a single homogeneous reactor with the a residence time similar to that of the whole burner rig using these two mechanisms.

Unlike the thermal nitric oxide chemistry, which was used to form the 166 species mechanism, the nitric oxide chemistry taken from the GRI mechanism contain species and reactions that interact with the rest of the combustion chemistry. It is in general not possible to combine mechanisms in this way without re-calibrating some reaction parameters and performing new validations, such a task is outside the scope of this thesis. To illustrate such interaction, Figure 23 shows a flow chart of the major reaction paths for the nitrogen atom for the steady state of a single homogeneous reactor with 20 mol-% hydrogen using the GRI mechanism. The residence time is long enough to give essentially complete combustion. The lower part of this chart shows reaction paths that involve hydrogen and carbon containing species. It was also seen that the trend in NO for the single homogeneous reactor is different from what is seen in the network: an almost linear increase with molar hydrogen content is seen, see Figure 22b.

4.4.6 Stochastic Reactor Networks

The central questions for the stochastic reactors is how many particles and what mixing time to use. To begin with it is important to clarify the different nature of these two parameters. The mixing time is a measure of how homogeneous the reactor is ($\tau \to 0$ corresponds to a homogeneous reactor). Mixing time is thus a physical quantity. Particle number on the other hand is a measure of the resolution of the PDF in a reactor in the numerical model; it is thus not a physical quantity and should ideally be as high as possible. A stochastic reactor with only one particle may behave just like a homogeneous reactor but this does not mean that use of low particle numbers makes the reactors more homogeneous in general. Using a low particle number just introduces discretization errors. The point is that a stochastic reactor with very few particles is expected to perform worse than a homogeneous reactor.

To determine how many particles are needed a parameter study was made. Network calculations were done for 100, 55, 40, 25, 15 and 5 particles per zone using the 28 species mechanism. The difference in temperature when going from 100 to 55 particles was no more than 30 K for any zone with most zones differing less than 15 K. Therefore the 100 particles case was used as reference. Differences in temperature compared to the other cases are shown in Figure 24a. Comparing with homogeneous reactor networks or computational fluid dynamics is not very informative since the mixing time estimate is not good enough. The comparison to computational fluid dynamics shown in Figure 24b clearly illustrates the discrepancy.

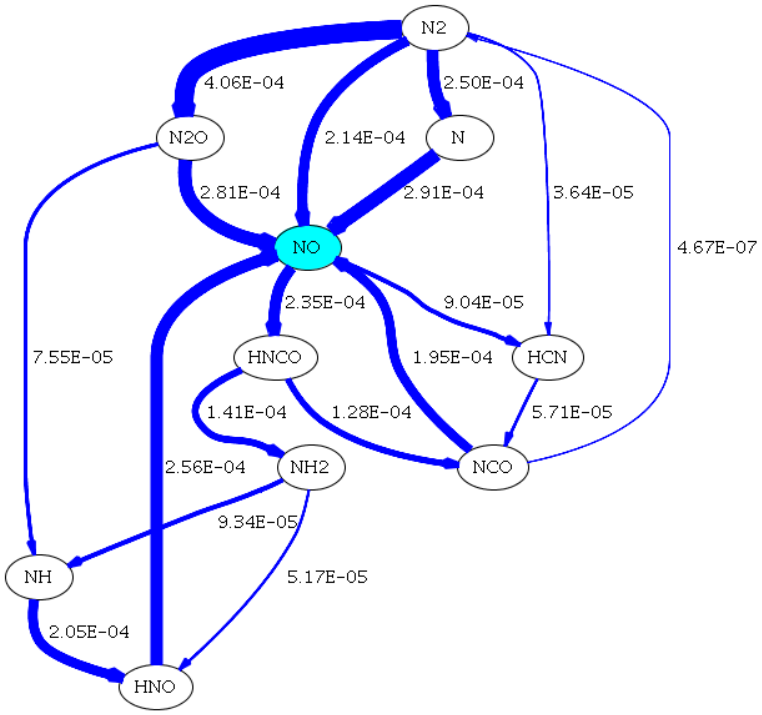

Figure 23: Flow chart for nitrogen atoms in a single homogeneous reactor using the GRI mechanism and 20 mol-% hydrogen. Numbers for flow rates are given in mol/s. Only net flow is shown.

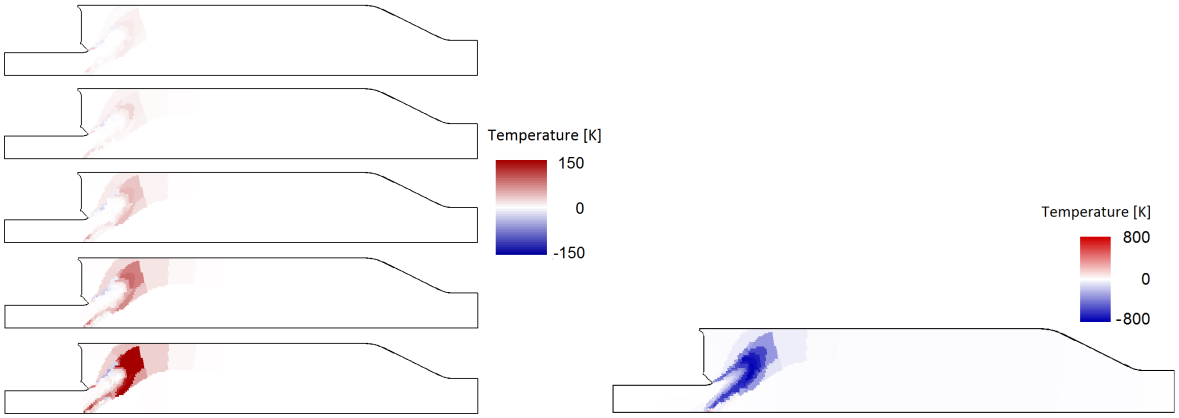

(a) **(b)**

Figure 24: (a) Temperature difference in [K] for stochastic reactor networks using 5 (bottom), 15, 25, 40 and 55 (top) particles per reactor compared to a network using 100 particles. The baseline network with 148 zones has been used. (b) Temperature difference between 100 particles per reactor network and the computational fluid dynamics simulation.

The optimum number of particles is evidently not the same for all zones. Having 100 particles in all zones is inefficient since CPU time scales with the total number of particles in the network. The 100 particle per reactor case had on average 143 000 particles total and took 10 hours to calculate on a single core. Before going to a more detailed mechanism an optimum number of particles should be selected for each zone.

The other central question is mixing time. To see the effect of the C_ϕ factor in equation (33), networks were calculated for a range of values: 1, 2, 10, 20 and 50. Figure 25 shows a comparison between the baseline computational fluid dynamics simulation (mass-weighted averages within each zone) and networks using these scaling factors, 55 particles per reactor and either Curl or modified Curl mixing model. Note that most of the error occurs due to under-predicted temperatures close to the flame region when the calculated flame position is pushed downstream. The mixing time in the modified Curl model is compensated as mentioned in section 2.5 so that one value of C_ϕ corresponds to the same variance decay rate in both models. Table 6 summarizes the largest positive and negative difference as well as the RMS difference between the networks and the computational fluid dynamics. The homogeneous reactor network is also included for comparison. RMS differences were calculated without any weighting because in the network all zones are considered equally important no matter their size. Best results are obtained around $C_\phi = 20$, the error increases for both more (higher C_ϕ) and less (lower C_ϕ) mixing. Modified Curl is better in all cases tested, which is consistent the continuous PDF produced by modified Curl as mentioned in [11].

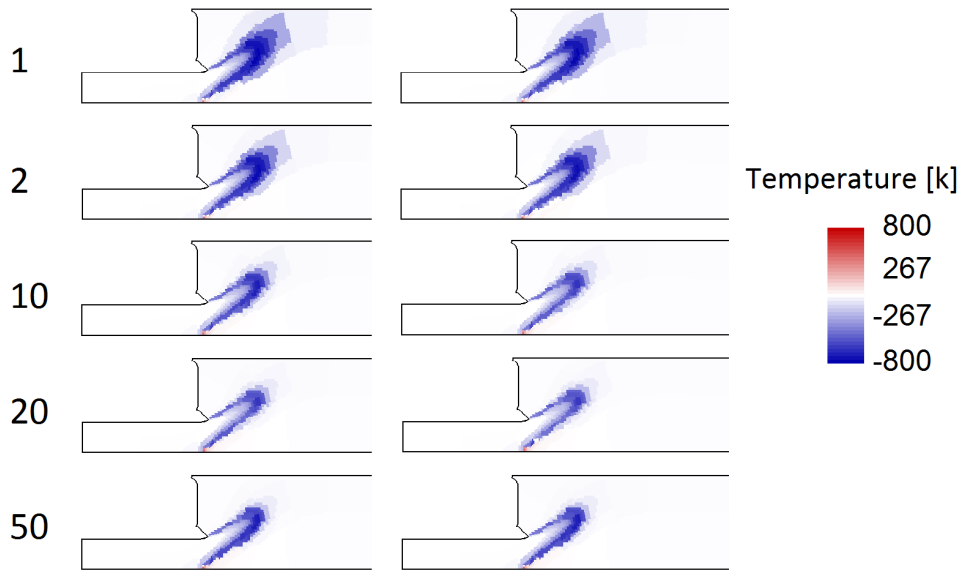

Figure 25: Temperature difference in [K] between computational fluid dynamics and stochastic reactor network simulations. Mixing time scale factor C_ϕ from top to bottom: 1, 2, 10, 20 and 50. Left: Curl mixing model. Right: Modified Curl mixing model.

4.5 Reactor Network Analysis of Sandia Flame D

A network based on the baseline homogeneous reactor computational fluid dynamics simulation of Sandia flame D was constructed with the cluster growth method. The tolerances are summarized in Table 7. The network has 133 zones and its geometry is shown in Figure 26.

Both homogeneous and stochastic reactor simulations give a flame too far downstream. Figure 27 shows the calculated temperature fields for homogeneous reactors and for stochastic

Table 6: Largest positive and negative difference and RMS difference between the stochastic networks and the baseline computational fluid dynamics simulation for Siemens burner rig.

Model	C_ϕ	Deviation [K]	
		min/max	RMS
Curl	1	+434 / -792	382
Modified Curl	1	+436 / -783	371
Curl	2	+449 / -773	363
Modified Curl	2	+456 / -764	353
Curl	10	+469 / -713	310
Modified Curl	10	+471 / -641	271
Curl	20	+471 / -635	262
Modified Curl	20	+472 / -624	249
Curl	50	+472 / -715	313
Modified Curl	50	+471 / -713	312
Homogeneous	-	+470 / -749	338

Table 7: Variables and tolerances used to construct the reactor network for Sandia flame D with the cluster growth method.

Variable	Tolerance
x and y coordinates	150 mm
y-velocity	20 m/s
Temperature	150 K
Density	0.15 kg/m^3
Mixture fraction	0.1
OH mass fraction	$2.0 \cdot 10^{-3}$
H_2O mass fraction	$1.5 \cdot 10^{-1}$
CO mass fraction	$1.0 \cdot 10^{-2}$

reactors using $C_\phi = 1$, 2 and 20. The downstream shift in the simulation is greater than for the Siemens burner rig. This is consistent with the hypothesis that the lack of separation between convection and turbulent transport causes the shift by reducing upstream transport. The Sandia flame does not have any recirculation making turbulent transport the only means of upstream transport.

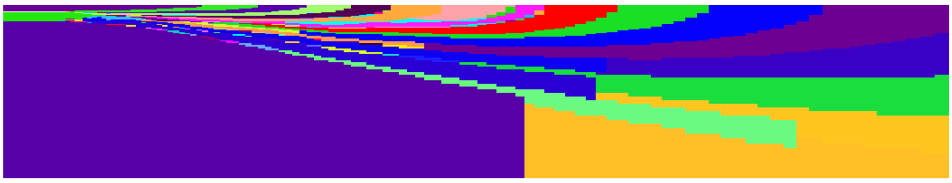

Figure 26: Reactor network geometry for Sandia flame D constructed with the cluster growth method.

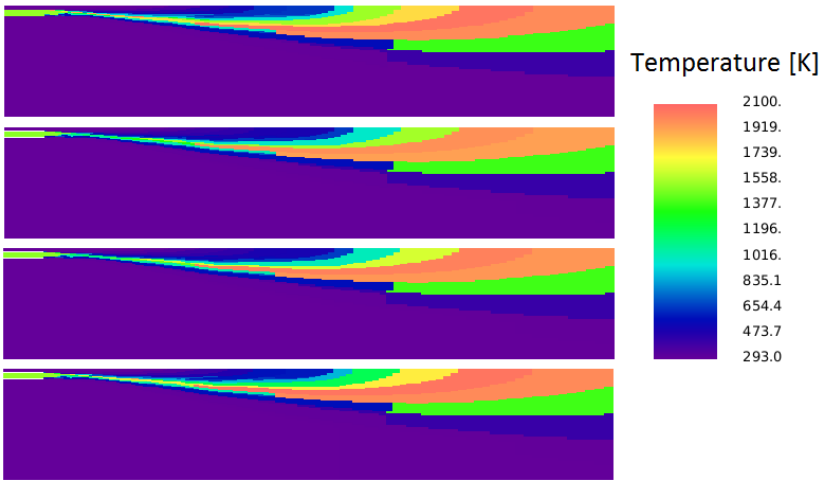

Figure 27: Temperature fields in [K] of Sandia flame D calculated with reactor networks. From top to bottom: homogeneous reactors, stochastic reactors with $C_\phi = 1$, 2 and 20.

5 Conclusions

Simulations of Sandia flame D and the Siemens burner rig have been performed with both computational fluid dynamics and reactor networks. For construction of reactor networks a new tool has been developed which utilizes a pre-calculated computational fluid dynamics solution to derive the network. The network construction tool has been applied to a Siemens burner rig and the network calculations show promising results in terms of temperature fields (compared to the computational fluid dynamics simulation) and NO trends (compared to experiments).

Computational fluid dynamics simulations of Sandia flame D were done using two different combustion models: homogeneous reactor and progress variable based CMC. The homogeneous reactor simulations show overall good agreement with the available experimental data although the flame is predicted to be a bit compressed and too hot. This compression may be a result of the turbulence model since it was seen that, when changing from the k-ε to the Reynolds stress turbulence model, the flame became a bit less compressed. When the combustion model was changed to progress variable based CMC the temperature dropped and the predicted maximum temperature was closer to the experimental. This is what is expected from a combustion model that does not assume perfect sub-grid mixing and indicates that the sub-grid distribution of states is important in this flame. The predicted flame was however even more compressed than in the homogeneous reactor case and a lift-off was falsely predicted. One likely reason for the lift-off is over-prediction of mixture fraction variance since extinction can more easily happen in regions of high variance. Possible causes of high variance is something that requires further investigation, for example by using a different turbulence model.

In computational fluid dynamics simulations of the Siemens burner rig it was observed that care must be taken to the inlet conditions: a constant velocity inlet lead to unstable flow with rapid oscillations. Using a constant mass flux inlet solved that problem. The NO level in homogeneous reactor simulations were of the right order of magnitude but lower than the experimental, a factor of 2 lower when using adiabatic walls and a factor of 3 when using fixed temperature walls, but it should be noted that prompt nitric oxide formation was not included in the chemical mechanism. Nitric oxides were not studied with the CMC model in this thesis. To do so a separate treatment of nitric oxide source terms would be needed because these minor species do not give a sizeable contribution to the progress variable. Natural extensions to the CMC calculations done in this thesis include a nitric oxide study, a study of the effect of mixture fraction variance at the inlets both for the burner rig and the Sandia D flame and further investigation of the Sandia flame series and the cause of the lift-off.

Two methods have been proposed for reactor network construction based on pre-calculated flow fields: a PCA-based method and a cluster growth method. Both methods construct a network by partitioning the mesh used for the computational fluid dynamics simulation into zones that fulfil given criteria on the spread of values of some field variables. It was found that the PCA method generally needs to create more zones to fulfil these criteria than the cluster growth method because the geometric connectivity check is separated from the initial partitioning which lead to larger amounts of small zones. Analysis of reactor networks was then performed with both homogeneous and stochastic reactors.

When making the tolerances for network construction stricter, and thus creating more zones, convergence was seen in all variables studied and results close to the computational fluid dynamics simulation were achieved for the Siemens burner rig. Temperature, emissions and flame position did however not converge to the exact values of the computational fluid dynamics simulation but a small offset was observed. It was also seen that the flame position was shifted downstream both for the Sandia D flame and the Siemens burner rig but the shift was much more prominent in the Sandia flame. A possible explanation for this discrepancy is that only

net flows were considered for each pair of cell faces when extracting the zone-to-zone flows. Turbulent transport, which can give a small flow in both directions across a cell face, was not separated from the convective flow, effectively reducing the upstream transport. This explanation is supported by the fact that the shift is smaller in the Siemens burner rig: in the rig the flame is stabilized by a central recirculation zone which makes turbulent transport less important for the flame position. In the Sandia flame, however, there is no recirculation present so turbulent transport is the only means of upstream transport. Treating the turbulent flux separately from the convective flux when extracting flows from the computational fluid dynamics solution and including both fluxes separately in the network may thus improve the results.

Reactor networks with a stochastic reactor in every zone were also studied. It was seen that the number of particles needed to predict the temperature field varies a lot between different zones, in the post flame no improvement was seen beyond 5 particles while in the flame front results were still improving up to the maximum of 100 particles that was tested. The modified Curl mixing model was found to consistently give slightly better results than the standard Curl mixing model. For a given network stochastic reactors overall gave results better than homogeneous reactors if the mixing time constant C_ϕ was around 20 but it is an open question how this constant is best estimated. Another unanswered question is if stochastic reactor networks can maintain accuracy with fewer reactors than a homogeneous network.

Calculation of NO emissions in reactor networks was done and the capability of a network to predict trends in NO for varying fuel composition without recalculating the flow with computational fluid dynamics was investigated. NO predictions depend heavily on the chemical reaction mechanism used. For the operating conditions studied it appears that both thermal and prompt NO formation are prominent. The trend of increasing NO with hydrogen enrichment of the fuel is reasonably predicted when prompt NO formation is included. To further study the effect of hydrogen enriched fuel in simulations and make quantitative predictions it is crucial to have a chemical mechanism which is validated for nitric oxide formation over the range of hydrogen contents used. The rig was mainly investigated using adiabatic walls due to uncertainty in heat losses. Estimating heat losses and including them in network calculations may also be a vital step to improve the prediction.

6 Outlook

In this section some suggestions that could be topics of future work are given.

- Further investigation of the LTIF-CMC model for the Sandia flames. For example comparing different turbulence models or using a large eddy simulation in order to find the cause of the lift-off. Using this model to predict trends when going from the D flame to the E and F flames represent the next step once the lift-off problem is solved.

- Measurement of heat losses in the Siemens burner rig and including them in the reactor network. It was seen in computational fluid dynamics simulations that even a slight heat loss affects the nitric oxide formation. Development and validation of a reaction mechanism for nitric oxide formation with hydrogen enriched fuel would also be required to improve nitric oxide predictions.

- Further development of the reactor network model. Most importantly, separating convective and turbulent transport and see if this solves the problem of flame fronts being shifted downstream. More elaborate network models could also be tested. For example, a conditional moment closure could be used for each reactor and the mass flows between zones made conditional on mixture fraction. This would effectively result in a network of

flamelets with conditional source terms due to mass flow. Another possibility would be to run a reactor network interactively with a computational fluid dynamics simulation and adapting the zones as the flow field changes in order to calculate non-stationary problems.

References

[1] A. H. Lefebvre and D.R. Ballal. *Gas turbine combustion: alternative fuels and emissions.* Boca Raton: Taylor and Francis., 2010.

[2] A. Lantz, R. Collin, M. Aldén, A. Lindholm, J. Larfeldt, and D. Lörstad. Investigation of hydrogen enriched natural gas flames in a SGT-700/800 burner using oh plif and chemiluminescence imaging. In *ASME Turbo Expo 2014: Turbine Technical Conference and Exposition*, GT2014-26293, 2014.

[3] N. Peters. *Turbulent combustion.* Cambridge monographs on mechanics and applied mathematics. Cambridge Univ. Press, 2000.

[4] T. Poinsot and D. Veynante. *Theoretical and numerical combustion.* Edwards, cop., 2001.

[5] CD-Adapco. *STAR-CD manual - Methodology, version 4.20*, 2013.

[6] A.Y. Klimenko and R.W. Bilger. Conditional moment closure for turbulent combustion. *Progress in Energy and Combustion Science*, 25(6):595–687, 1999.

[7] H. Lehtiniemi, A. Borg, and F. Mauss. Conditional moment closure with a progress variable approach. In *Proceedings of the 8th International Conference on Modeling and Diagnostics for Advanced Engine Systems.* COMODIA, 2012.

[8] H. Lehtiniemi. *Development of transient flamelet library based combustion models.* PhD thesis, Division of Combustion Physics, Department of Physics, Lund University, 2013.

[9] S.B. Pope. PDF methods for turbulent reactive flows. *Progress in energy and combustion science*, 11:119–192, 1985.

[10] D. W. Meyer and P. Jenny. Micromixing models for turbulent flows. *Journal of Computational Physics*, 228:1275–1293, 2008.

[11] D.C. Haworth. Progress in probability density function methods for turbulent reacting flows. *Progress in Energy and Combustion Science*, 36:168–259, 2009.

[12] S.B. Pope. Small scales, many species and the manifold challenges of turbulent combustion. *Proceedings of the Combustion Institute*, 34:1–31, 2013.

[13] J. Frank R. Barlow. Piloted CH4/air flames C, D, E and F - release 2.1, http://www.ca.sandia.gov/TNF. Technical report, Sandia National Laboratories, 2007.

[14] D. Lörstad, A. Lindholm, J. Pettersson, M. Björkman, and I. Hultmark. Siemens SGT-800 industrial gas turbine enhanced to 50 MW: Combustor design modifications, validation and operation experience. In *ASME Turbo Expo 2013: Power for Land, Sea and Air*, GT2013-95478, 2013.

[15] D. Lörstad, W. Lieke, S. Axelsson, and M. Björkman. Siemens gas turbine SGT-800 enhanced to 50 MW: Design modifications, validation and operation experience. In *Proc. PowerGen Europe*, 2013.

[16] J Xu and SB Pope. PDF calculations of turbulent nonpremixed flames with local extinction. *Combustion and flame*, 123(3):281 – 307, 2000.

[17] A. Garmory and E. Mastorakos. Sensitivity analysis of LES-CMC predictions of piloted jet flames. *International Journal of Heat and Fluid Flow*, 39:53–63, 2013.

[18] S.A. Ferraris and J.X. Wen. LES of the Sandia flame D using laminar flamelet decomposition for conditional source-term estimation. *Flow, Turbulence and Combustion*, 81(4):609–639, 2008.

[19] M Ihme and H Pitsch. Prediction of extinction and reignition in nonpremixed turbulent flames using a flamelet/progress variable model 2. application in LES of Sandia flames D and E. *Combustion and flame*, 155(1-2):90 – 107, 2008.

[20] E.A. Brizuela and M.Z. Roudsari. Comparison of RANS/CMC modeling of flame D with conventional and with presumed mapping function statistics. *Combustion Theory and Modelling*, 15(5):671–690, 2011.

[21] D. Lörstad, A. Lindholm, A. Lantz, R. Collin, M. Aldén, N. Alin, and C. Fureby. Experimental and LES investigation of a SGT-800 burner in a combustion rig. In *ASME Turbo Expo 2010: Power for land, sea and air*, GT2010-22688, 2010.

[22] D. Lörstad, A. Lindholm, D. G. Barhaghi, A. Bonaldo, A. Lantz, R. Collin, M. Aldén, E. Fedina, and C. Fureby. Measurements and LES of a SGT-800 burner in a combustion rig. In *ASME Turbo Expo 2012: Power for land, sea and air*, GT2012-69936, 2012.

[23] S. Bruneflod. Flow simulations of an axisymmetric two-dimensional 3:rd generation DLE burner. Master's thesis, Department of applied physics a mechanical engineering, Luleå University of Technology, 2010.

[24] N Hamedi. Numerical study of NOx and flame shape of a DLE burner. Master's thesis, Department of Management and Engineering, Linköping University, 2012.

[25] S. Sepideh Marashi. Network modeling application to laminar flame speed and NOx prediction in industrial gas turbines. Master's thesis, Department of Management and Engineering, Linköping University, 2013.

[26] O. Bosyi. Simulation of a gas turbine combustor test rig using a reactor network approach with detailed chemistry. Master's thesis, Thermodynamics and Thermal Process Engineering, Brandenburg University of Technology Cottbus Senftenberg, 2014.

[27] V. Fichet, M. Kanniche, P. Plion, and O. Gicquel. A reactor network model for predicting NOx emissions in gas turbines. *Fuel*, 89(9):2202–2210, 2010.

[28] M. Falcitelli, L. Tognotti, and S. Pasini. An algorithm for extracting chemical reactor network models from CFD simulation of industrial combustion systems. *Combustion Science and Technology*, 174(11-12):27–42, 2002.

[29] S.A. Drennan. Flow field derived equivalent reactor networks for accurate chemistry simulation in gas turbine combustors. In *AMSE Turbo Expo 2009: Power for land, sean and air*, GT2009-59861, 2009.

[30] M. Schenk, K. Moshammer, P. Osswald, K. Kohse-Höinghaus, L. Leon, L. Seidel, F. Mauss, and T. Zeuch. Detailed mass spectrometric and modeling study of isomeric butene flames. *Combustion and Flame*, 160(3):487–503, 2013.

[31] G. P. Smith, D. M. Golden, M. Frenklach, N. W. Moriarty, B. Eiteneer, M. Goldenberg, C. T. Bowman, R. K. Hanson, S. Song, W. C. Gardiner, V. V. Lissianski, and Z. Qin. GRI-Mech 3.0, http://www.me.berkeley.edu/gri_mech, 2014.

[32] LOGE AB. LOGEsoft, http://www.loge.se/products/loge_products.html, 2014.

[33] M. Jangi, X. Zhao, D. C. Haworth, and X. Bai. Stabilization and liftoff length of a non-premixed methane/air jet flame discharging into a high-temperature environment: An accelerated transported pdf method. *Combustion and Flame. In press*, 2014.

[34] R. S. Barlow and A. N. Karpetis. Measurements of scalar variance, scalar dissipation, and length scales in turbulent piloted methane/air jet flames. *Flow, turbulence and combustion*, 72:427–448, 2004.